

# SYNTHESIS, CHARACTERIZATION AND STUDIES ON OPTICAL PROPERTIES OF ZnS-SiO<sub>2</sub> NANOCOMPOSITES

## A DISSERTATION

*Submitted in partial fulfillment of the  
requirements for the award of the degree*

*of*

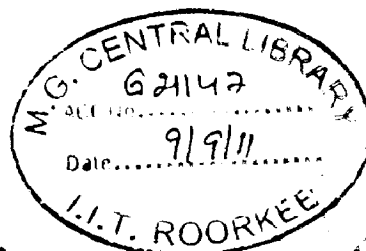
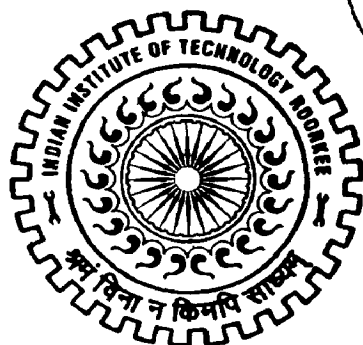
MASTER OF TECHNOLOGY

*in*

NANOTECHNOLOGY

*By*

**HIMANSHU SEKHAR MAHARANA**



CENTRE OF NANOTECHNOLOGY  
INDIAN INSTITUTE OF TECHNOLOGY ROORKEE  
ROORKEE - 247 667 (INDIA)

JUNE, 2011

Indian Institute of Technology Roorkee

Centre of Nanotechnology

**CANDIDATE'S DECLARATION**

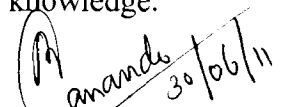
I hereby declare that the work which is being presented in the dissertation named **“SYNTHESIS, CHARACTERIZATION AND STUDIES ON OPTICAL PROPERTIES OF ZnS-SiO<sub>2</sub> NANOCOMPOSITES”** in partial fulfillment of the requirements for the award of the degree of Master of Technology submitted in the Centre of Nanotechnology, IIT Roorkee is an authentic record of my own work carried out during the period of August, 2010 to June, 2011 under the supervision and guidance of **Dr. P. Jeevanandam**.

The matter embodied in this project work has not been submitted for the award of any other degree.

Date..... 30.06.2011

Himanshu Sekhar Maharana  
(Himanshu Sekhar Maharana)

This is to certify that the above statement made by the candidate is correct to the best of my knowledge.

  
(Dr. P. Jeevanandam)

Asst. Professor

Dept. of Chemistry & Centre of Nanotechnology

Indian Institute of Technology Roorkee

Roorkee-247667

## **Acknowledgements**

I feel honored in expressing my deepest sense of gratitude to my guide, Dr. P.Jeevanandam, for providing me the opportunity to carry out research under his able guidance. His exceptional capability of reducing complexities in to simpler form has enormously helped me in the smooth progress of the work. It is the implementation of his ideas and work plan that has led to meaningful results and conclusions. Without his encouragement and guidance, I could not have finished my thesis work.

I want to thank Prof. Anil Kumar, Head, Centre of Nanotechnology for his kind help. It is a time to say a lot of thanks to Mr. Nagaratna Kishore, who always assisted me like as an elder brother during my experimental work and discussion on the thesis work. He always encouraged me to do the best. I really gained a lot of knowledge from the discussions I had with him.

I can not forget the efforts put in by Miss Manu Sharma throughout my M.Tech dissertation work.

I would like to thank Miss Geetu Sharma and Miss Nisha bayal for their help through out the experimental work. It was a great pleasure to work with them

I would like to thank my friends for helping and encouraging me time to time during my whole M.Tech and every difficult situation of my life.

Really, the acknowledgement is incomplete without saying something about my family. It is my pleasant duty to recall with gratitude the everlasting affection, unconditional love,

encouragement and all sorts of supports and last but not the least to say a lot of thanks to the staff of Center Of Nanotechnology for helping me time to time during my whole duration of M.Tech.

Finally, I would like to thank God and all those who have helped me directly or indirectly in completing my thesis.

I.I.T ROORKEE

Himanshu Sekhar Maharana

June 2011

## ***ABSTRACT***

Nanocomposite consists of a matrix to which nanoparticles are added to improve a particular material property such as electrical conductivity, optical clarity, thermal stability, etc. ZnS-SiO<sub>2</sub> nanocomposite is widely used in electronic devices, specifically, in light emitting diodes and also in biological labeling due to its excellent photo stability. ZnS-SiO<sub>2</sub> nanocomposites have been synthesized by different methods such as Rf sputtering, micro-emulsion and wet chemical method. Most of these methods are costly and complex. In the present study, a simple sol-gel synthesis of ZnS-SiO<sub>2</sub> nanocomposite has been investigated. In the sol-gel method, the chemical elements become uniformly distributed during gel formation and production of ultrafine particle with small crystallite size at lower temperature can be achieved. For the synthesis of ZnS-SiO<sub>2</sub> nanocomposites, zinc acetate and thioacetamide were taken in 1:1 molar ratio and then a mixture of ethanol, toluene and tetraethyl orthosilicate were added. This was followed by the addition of ammonia solution along with a small amount of distilled water. The obtained gel was dried at 80°C. Mn doped ZnS-SiO<sub>2</sub> nanocomposites were also obtained by the same procedure by adding zinc acetate and manganese acetate with different mole ratios (90:10, 95:05, 98:02). The XRD patterns of the composites showed peaks due to only ZnS because SiO<sub>2</sub> is amorphous. The DRS spectra of the composites showed the characteristic absorption bands of ZnS-SiO<sub>2</sub>. In Mn doped ZnS-SiO<sub>2</sub> nanocomposites, the band gap increased in comparison to pure ZnS and ZnS-SiO<sub>2</sub> nanocomposites. FE-SEM images of ZnS-SiO<sub>2</sub> and Mn doped ZnS-SiO<sub>2</sub> nanocomposites showed agglomeration of spherical shaped nanoparticles. EDXA analysis also confirmed the presence of elements (Zn, S, O, Mn and Si). The photoluminescence spectra of ZnS-SiO<sub>2</sub> nanocomposites showed the emission bands of ZnS. The present method is an easy method to synthesize ZnS-SiO<sub>2</sub> and Mn doped ZnS-SiO<sub>2</sub> nanocomposites at low temperature.

## *Abbreviation*

FE-SEM = Field emission scanning electron microscope

FT-IR = Fourier transform infrared spectroscopy

EDXA = Energy dispersive X-ray analysis

TAA = Thioacetamide

TEOS = Tetraethyl orthosilicate

PL = Photoluminescence

DRS = Diffuse reflectance spectra

TGA = Thermal gravimetric analysis

RT = Room temperature

## TABLE OF CONTENTS

	Page number
<b>Candidate's Declaration</b>	<b>i</b>
<b>Acknowledgements</b>	<b>ii</b>
<b>Abstract</b>	<b>iv</b>
<b>Abbreviation</b>	<b>v</b>
<b>Table of Contents</b>	<b>vi</b>
<b>List of Figures</b>	<b>x</b>
<b>1 INTRODUCTION</b>	
<b>1.1 Introduction</b>	<b>1</b>
<b>1.2 How Nanocomposite Work?</b>	<b>2</b>
<b>1.3 Types of Nanocomposites</b>	<b>2</b>
<b>1.3.1 Ceramic Nanocomposites</b>	<b>2</b>
<b>1.3.2 Metal Nanocomposites</b>	<b>3</b>

<b>1.3.3 Polymer Nanocomposites</b>	<b>3</b>
<b>1.3.4 Magnetic Nanocomposites</b>	<b>5</b>
<b>1.4 Improved Properties of Nanocomposites</b>	<b>7</b>
<b>1.5 Applications</b>	<b>7</b>
<b>1.5.1 Oxygen and Gas Barrier</b>	<b>8</b>
<b>1.5.2 Food Packaging</b>	<b>9</b>
<b>1.5.3 Fuel Tanks</b>	<b>9</b>
<b>1.5.4 Transparent Films</b>	<b>10</b>
<b>1.5.5 Environmental Protection</b>	<b>10</b>
<b>1.5.6 Flammability Reduction</b>	<b>11</b>
<b>1.6 Scope of Present Study</b>	<b>12</b>
<b>2 EXPERIMENTAL METHODS</b>	<b>13</b>
<b>2.1 Materials</b>	<b>13</b>
<b>2.2 Equipment</b>	<b>13</b>
<b>2.2.1 X-ray diffractometer</b>	<b>13</b>
<b>2.2.2 Infrared spectroscopy</b>	<b>14</b>
<b>2.2.3 FE-SEM coupled with EDXA</b>	<b>14</b>



2.2.4	Diffuse reflectance spectroscopy	15
2.2.5	Fluorescence spectroscopy	16
2.2.6	Thermal gravimetric analysis	16
2.3	Methodology	17
2.3.1	Scheme-1	18
2.3.2	Scheme-2	19
3	RESULTS AND DISCUSSION: ZnS-SiO <sub>2</sub> NANOCOMPOSITES	21
3.1	XRD analysis of ZnS-SiO <sub>2</sub> nanocomposites	21
3.2	FE-SEM images and EDXA analysis of ZnS-SiO <sub>2</sub> nanocomposites	23
3.3	FT-IR analysis of ZnS-SiO <sub>2</sub> nanocomposites	29
3.4	Thermal gravimetric analysis of ZnS-SiO <sub>2</sub> nanocomposites	31
3.5	Diffuse reflectance spectral analysis of ZnS-SiO <sub>2</sub> nanocomposites	32
3.6	Photoluminescence spectra of ZnS nanoparticles and ZnS-SiO <sub>2</sub> nanocomposites	35
4	Mn DOPED ZnS-SiO <sub>2</sub> NANOCOMPOSITES	37
4.1	XRD analysis of Mn doped ZnS-SiO <sub>2</sub> nanocomposites	37
4.2	FE-SEM images and EDXA analysis of Mn doped ZnS-SiO <sub>2</sub>	

<b>nanocomposites</b>	<b>40</b>
<b>4.3 FT-IR analysis of Mn doped ZnS-SiO<sub>2</sub> nanocomposites</b>	<b>45</b>
<b>4.4 Thermal gravimetric analysis of Mn doped ZnS-SiO<sub>2</sub> nanocomposites</b>	<b>46</b>
<b>4.5 Diffuse reflectance spectral analysis of Mn doped ZnS-SiO<sub>2</sub> nanocomposites</b>	<b>47</b>
<b>4.6 PL spectra Mn doped ZnS-SiO<sub>2</sub> nanocomposites</b>	<b>50</b>
<b>5 CONCLUSIONS</b>	<b>53</b>
<b>REFERENCES</b>	<b>54</b>

## LIST OF FIGURES

Sl.No.	NAME OF FIGURES	PAGE NO
1.1	Polymer nanocomposite	4
1.2	Magnetic nanocomposite technology	6
1.3	Flame reduction using nanocomposite	11
3.1.1	XRD analysis of Zn-SiO <sub>2</sub> nanocomposites	22
3.1.2	XRD analysis of ZnS-SiO <sub>2</sub> nanocomposites calcined at 400°C	23
3.2.1	FE-SEM images of pure ZnS, SiO <sub>2</sub> nanoparticles and ZnS-SiO <sub>2</sub> nanocomposites	24
3.2.2	FE-SEM images of ZnS-SiO <sub>2</sub> nanocomposites calcined at 400°C	25
3.2.3	EDXA data of pure ZnS, SiO <sub>2</sub> and ZnS-SiO <sub>2</sub> nanocomposites	26-28
3.3.1	FT-IR analysis of pure SiO <sub>2</sub> nanoparticle	29
3.3.2	FT-IR analysis of pure ZnS nanoparticles and ZnS-SiO <sub>2</sub> nanocomposites	30
3.4.1	TGA analysis of ZnS-SiO <sub>2</sub> nanocomposites	31
3.5.1	DRS spectra of pure ZnS and ZnS-SiO <sub>2</sub> nanocomposites	33

3.5.2	Estimation of band gap from the DRS spectra of ZnS-SiO <sub>2</sub> nanocomposites	34
3.6.1	Photoluminescence spectra of ZnS nanoparticles and ZnS-SiO <sub>2</sub> nanocomposites	35
3.6.2	PL spectra of ZnS-SiO <sub>2</sub> nanocomposites calcined at 400°C	36
4.1.1	XRD analysis of Mn doped ZnS-SiO <sub>2</sub> nanocomposites	38
4.1.2	XRD analysis of Mn doped ZnS-SiO <sub>2</sub> nanocomposites calcined at 400°C	39
4.2.1	FE-SEM images of Mn doped ZnS-SiO <sub>2</sub> nanocomposites	41
4.2.2	FE-SEM images of Mn doped ZnS-SiO <sub>2</sub> nanocomposites calcined at 400°C	42
4.2.3	EDXA data of Mn doped ZnS-SiO <sub>2</sub> nanocomposites	43
4.3.1	FT-IR analysis of Mn doped ZnS-SiO <sub>2</sub> nanocomposites	45
4.4.1	TGA analysis of Mn doped ZnS-SiO <sub>2</sub> nanocomposites	46
4.5.1	DRS spectra of Mn doped ZnS-SiO <sub>2</sub> nanocomposites	48
4.5.2	Estimation of band gap from the DRS spectra of Mn doped ZnS-SiO <sub>2</sub> nanocomposites	49
4.6.1	Photoluminescence spectra of Mn doped ZnS-SiO <sub>2</sub> nanocomposites	51
4.6.2	PL spectra of Mn doped ZnS-SiO <sub>2</sub> nanocomposites calcined at 400°C	52



*Chapter 1*

*Introduction*

# CHAPTER 1

## ***1.1 Introduction:***

Nanocomposite materials are formed by mixing two or more dissimilar materials at the nanoscale in order to control and develop new and improved structures and properties. A nanocomposite is a multiphase solid material where one of the phases has one, two or three dimensions of less than 100 nanometer (nm), or structures having nano-scale repeat distances between the different phases that make up the material [1].

The properties of nanocomposites depend not only upon the individual components used but also upon the morphology and the interfacial characteristics. Nanocomposite coatings and materials are among the most exciting and fastest-growing areas of research. With new materials being continually developed, they often exhibit novel properties that are absent in the constituent materials. Nanocomposite materials have enormous potential for new applications including: aerospace, automotive, electronics, biomedical implants, non-linear optics, mechanically reinforced lightweight materials, sensors, nanowires, batteries, bioceramics, energy conversion and many others [2].

The mechanical, electrical, thermal, optical, electrochemical and catalytic properties of the nanocomposites differ markedly from that of the component materials. Size limits for these effects have been proposed [3], i.e. particle size  $< 5$  nm for catalytic activity,  $< 20$  nm for making a hard magnetic material soft,  $< 50$  nm for refractive index changes, and  $< 100$  nm for achieving superparamagnetism.

## ***1.2 How Nanocomposites Work?***

Nanoparticles have extremely high surface to volume ratio which dramatically changes their properties when compared with their bulk sized particles. It also changes the way in which the nanoparticles bond with the bulk material. The result is that the composite can be many times improved with respect to the component parts. Some nanocomposite materials have been shown to be 1000 times tougher than the bulk component materials.

## ***1.3 Types of Nanocomposites***

The important types of nanocomposites are:

- Ceramic nanocomposites
- Metal nanocomposites
- Polymer nanocomposites
- Magnetic nanocomposites

### ***1.3.1 Ceramic Nanocomposites***

In ceramic nanocomposites, the main part of the volume is occupied by a ceramic, i.e. a chemical compound from the group of oxides, nitrides, borides, etc. In most cases, the ceramic nanocomposites contain a metal as the second component. Ideally, both the components (metallic one and the ceramic one) are finely dispersed in each other in order to explore a particular property. Nanocomposites from these have been demonstrated in improving their optical, electrical and magnetic properties [4] as well as biological, corrosion-resistance and other protective properties [5].

The phase diagram of the mixture should be considered in designing ceramic-metal nanocomposites and measures have to be taken to avoid a chemical reaction between both the components. The last point is mainly important for the metallic component that may easily react with the ceramic and thereby loses its metallic character. It should be noted that the preparation of the ceramic component generally requires high process temperatures.

The concept of ceramic-matrix nanocomposites was also applied to thin films that are solid layers of a few nm to some tens of  $\mu\text{m}$  thickness deposited upon a substrate and that play an important role in the functionalization of surfaces. Gas flow sputtering by the hollow cathode technique turned out as a rather effective technique for the preparation of nanocomposite layers [6,7]. The process operates as a vacuum-based deposition technique and is associated with high deposition rates up to some  $\mu\text{m}$  and the growth of nanoparticles in the gas phase. Nanocomposite layers in the ceramics range of composition were prepared from  $\text{TiO}_2$  and Cu by the hollow cathode technique [8]. The composites showed high mechanical hardness, small coefficients of friction and a high resistance to corrosion.

### ***1.3.2 Metal Nanocomposites***

Another kind of nanocomposite is the energetic nanocomposite. Metal oxides when combined with nano scale aluminium powder can form super thermite materials [9-11].

### ***1.3.3 Polymer Nanocomposites***

In this case, appropriately added nanoparticulates to a polymer matrix can enhance its performance by simply capitalizing on the nature and properties of the nanoscale filler (these materials are better described by the term nanofilled polymer composites) [12]. This strategy is



particularly effective in yielding high performance composites, when good dispersion of the filler is achieved and the properties of the nanoscale filler are substantially different or better than those of the matrix, for example, reinforcing a polymer matrix by much stiffer nanoparticles of ceramics, clays (Fig 1.1), or carbon nanotubes [13, 14]. Alternatively, the enhanced properties of high performance nanocomposites may be mainly due to the high aspect ratio and high surface area of the fillers [15, 16]. Since nanoparticles have extremely high surface area to volume ratios, good dispersion can be achieved.

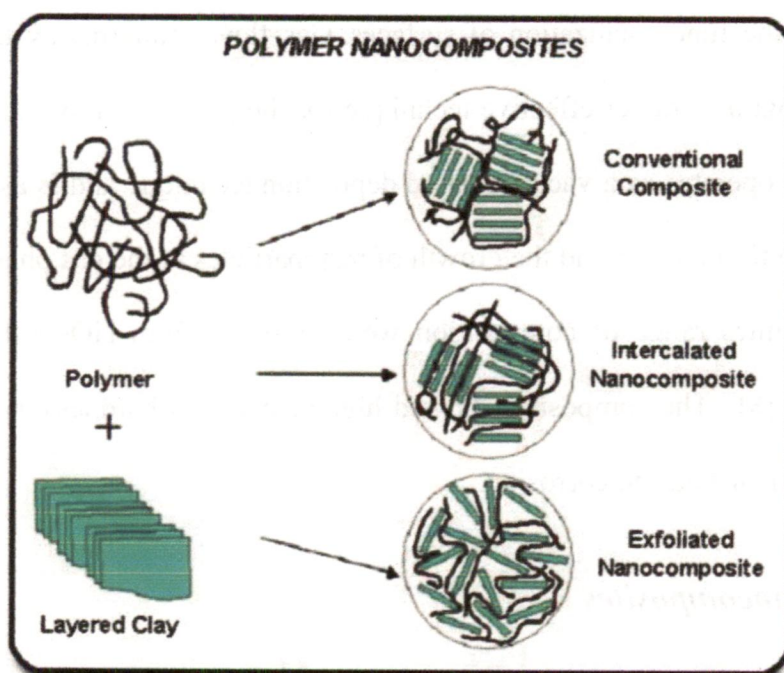


Fig 1.1: Polymer nanocomposites formed from a layered clay and a polymer [18, 19]

Nanoscale dispersion of fillers or controlled nanostructures in the composite can introduce new physical properties and novel behaviour that are absent in the unfilled matrices, effectively changing the nature of the original matrix (such composite materials can be better described by the term genuine nanocomposites or hybrids) [12]. Some examples of such new properties are fire resistance or flame retardancy and accelerated biodegradability [17].

#### ***1.3.4 Magnetic Nanocomposites:***

Magnetic materials have been playing a key role for the miniaturization of electronic equipment. Inductive components are extensively used in high frequency ( $> 1$  MHz) electronic devices such as radar, satellite, telecommunication systems and home radios. Conventional inductive components use metallic alloys and ferrites as core materials. The major problem for metallic materials is their low resistivity. Since it is impossible to dramatically increase their resistivity, metallic materials were excluded in high frequency applications and ferrites have been the only choice. Although efforts have been made to improve the performance of the ferrites, very limited progress was made [20, 21].

To overcome the difficulties of both metallic alloys and ferrites, metals or ceramic nanocomposites are the next generation materials for high frequency magnetic applications. The nanocomposite processing has provided a new approach for fabricating soft magnetic materials. In a magnetic or ceramic nanocomposite, the resistivity can be drastically increased, leading to significantly reduced eddy current loss. In addition, the exchange coupling between neighboring magnetic nanoparticles can overcome the anisotropy and demagnetizing effect, resulting in much better soft magnetic properties than the conventional bulk materials (Fig.1.2).

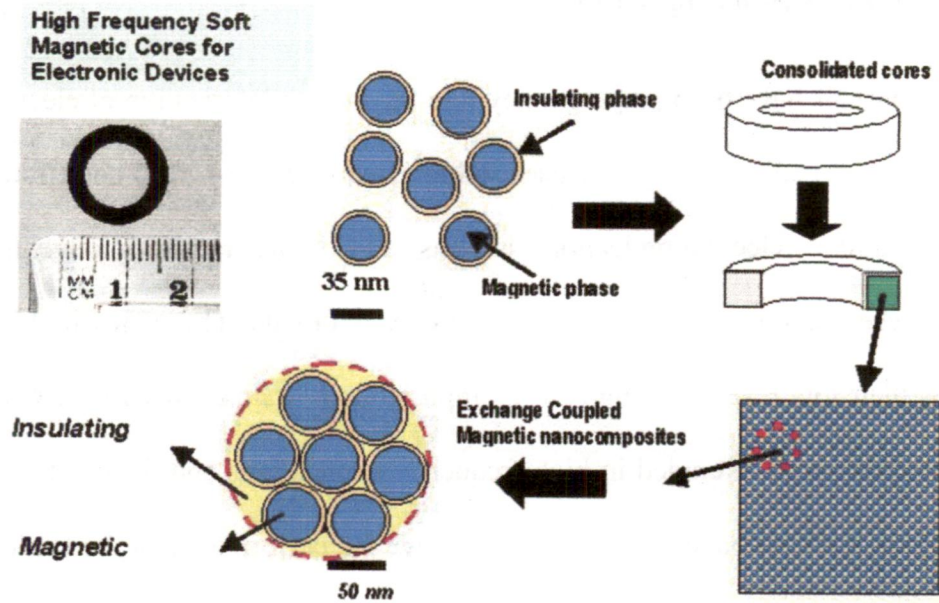


Fig. 1.2: Schematic representation of magnetic nanocomposite technology [22]

In the recent times, the following research areas are important with regard to magnetic nanocomposites.

- Chemical synthesis of Ni-Fe/SiO<sub>2</sub>, Co/SiO<sub>2</sub>, Fe-Co/SiO<sub>2</sub>, Fe/nickel-ferrite, Ni-Zn-ferrite/SiO<sub>2</sub>, Fe-Ni/ polymer, and Co/polymer magnetic nanocomposites [23].
- Consolidate the magnetic nanocomposite powders into exchange coupled (> 90% theoretical density) bulk components via vacuum hot press consolidation or tape casting process [22, 23].
- Performance evaluation of the exchange coupled magnetic nanocomposite components.

### ***1.4 Improved Properties of Nanocomposites:***

Nanocomposites can dramatically improve properties like:

- Mechanical properties including strength, modulus and dimensional stability
- Electrical conductivity
- Decreased gas, water and hydrocarbon permeability
- Flame retardancy
- Thermal stability
- Chemical resistance
- Surface appearance
- Optical clarity

### ***1.5 Applications***

Nanocomposites are currently used in a number of fields and new applications are being developed. The applications of nanocomposites include:

- Thin-film capacitors for computer chips
- Solid polymer electrolytes for batteries
- Automotive engine parts and fuel tanks
- Impellers and blades
- Oxygen and gas barriers
- Food packaging

The improvements in properties have resulted in major interest in nanocomposite materials in numerous automotive, general and industrial applications. These include potential for utilisation as mirror housings on various vehicle types, door handles, engine covers and intake manifolds and timing belt covers. More general applications currently being considered include usage as impellers and blades for vacuum cleaners, power tool housings and covers for portable electronic equipment such as mobile phones, pagers, etc. Some of the interesting applications have been described below.

### ***1.5.1 Oxygen and Gas Barriers***

The gaseous barrier property improvement that can result from relatively small quantities of nanoclay materials is shown to be substantial. Data provided from various sources indicate that oxygen transmission rates for polyamide-organoclay composites are usually less than half of that of the unmodified polymer. Further data reveals the extent to which both the amount of clay incorporated in the polymer and the aspect ratio of the filler contributes to overall barrier performance [24]. In particular, aspect ratio is shown to have a major effect, with high ratios quite dramatically enhancing gaseous barrier properties.

Honeywell [25] has been active in developing a combined active or passive oxygen barrier system based on polyamide-6 materials. Passive barrier characteristics are provided by nanoclay particles incorporated via melt processing techniques while the active contribution comes from an oxygen scavenging ingredient. Oxygen transmission results reveal substantial benefits provided by nanoclay in comparison to the base polymer (rates approximately 15-20% of the bulk polymer value, with further benefits provided by the combined active or passive system). It is suggested that the increased torsion provided by the nanoclay particles essentially slows

transmission of oxygen through the composite and drives molecules to the active scavenging species resulting in near zero oxygen transmission for a considerable period of time.

### ***1.5.2 Food Packaging***

Currently there is requirement for a non refrigerated packaging system capable of maintaining food freshness for a long time [26]. Nanoclay polymer composites are currently showing considerable promise for this application. The excellent barrier characteristics of these composites have resulted in considerable interest in nanoclay composites in food packaging applications. Specific examples include packaging for processed meats, cheese, confectionery and boil-in-the-bag foods, extrusion-coating applications in association with paper board for fruit juice and dairy products and also co-extrusion processes for the manufacture of beer and carbonated drinks bottles. The use of nanocomposite formulations would be expected to enhance considerably the expiry time of many types of food.

### ***1.5.3 Fuel Tanks***

The ability of nanoclay incorporation to reduce solvent transmission through polymers such as polyamides has been demonstrated [27]. Significant reduction in fuel transmission through polyamide 6/66 polymers by incorporation of a nanoclay filler has been noticed [28]. As a result, considerable interest is now being shown in these materials as both fuel tank and fuel line components for cars. Of further interest for this type of application, the reduced fuel transmission characteristics are accompanied by significant material cost reductions.

#### ***1.5.4 Transparent Films***

The presence of filler at nano-levels has also been shown to have significant effects on the transparency characteristics of films. In comparison to conventionally filled polymers, nanoclay has been shown to significantly enhance the transparency [29]. With polyamide based composites, this effect has been shown to be due to modifications in the crystallisation behaviour brought about by the nanoclay particles; spherulitic domain dimensions being considerably smaller. Similarly, nano-modified polymers have been shown, when employed to coat polymeric transparency materials, to enhance both toughness and hardness of these materials without interfering with the light transmission characteristics. The ability to resist high velocity impact combined with substantially improved resistance has also been investigated [30, 31].

#### ***1.5.5 Environmental Protection***

Water laden atmospheres have long been regarded as one of the most damaging environments which polymeric materials can encounter. Thus an ability to minimise the extent to which water is absorbed can be a major advantage. Nanoclay incorporation can reduce the extent of water absorption in a polymer [32, 33]. Similar effects have been observed with polyamide based nanocomposites. In addition a significant effect of nanoclay aspect ratio on water diffusion characteristics in polyimide nanocomposites have been observed. Specifically, increasing aspect ratio was found to diminish substantially the amount of water absorbed, thus indicating the beneficial effects likely from nanoparticles in comparison to conventional microparticle loading. Hydrophobic enhancement would clearly promote both improved nanocomposite properties and diminish the extent to which water would be transmitted through to an underlying substrate. Thus applications in which contact with water or moist environments are likely could clearly benefit from materials incorporating nanoclay particles.

### ***1.5.6 Flammability Reduction***

The ability of nanoclay incorporation to reduce the flammability of polymeric materials was a major theme of the paper published by Gilman et al [34, 35]. Gilman et al. have demonstrated the extent to which flammability behaviour could be restricted in polymers such as polypropylene with as little as 2% nanoclay loading. In particular, heat release rates, as obtained from cone calorimetry experiments (Fig.1.3), were found to diminish substantially by nanoclay incorporation. Although conventional microparticle filler incorporation together with the use of flame retardant would also minimise flammability behaviour, this is usually accompanied by reduction in various other important properties. With the nanoclay approach, this is usually achieved while maintaining or enhancing other properties and characteristics.

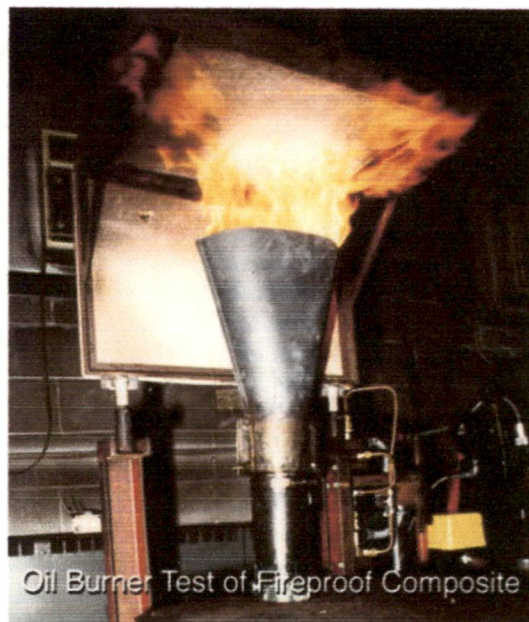


Fig. 1.3: Flame reduction using a nanocomposite [17]



### ***1.6 Scope of present study:***

ZnS is well-known direct band gap semiconductor with a bandgap of 3.77eV. It is a promising material for fabricating optical and electronics devices. SiO<sub>2</sub> is chemically inert and optically transparent. When SiO<sub>2</sub> is mixed with ZnS it may enhance the optical properties of the material which is very much useful in house hold and industrial applications. ZnS-SiO<sub>2</sub> can be prepared using a variety of chemical methods but these methods are complex and time consuming. In the present work, ZnS-SiO<sub>2</sub> nanocomposites were prepared using a simple sol-gel approach. Manganese doped ZnS-SiO<sub>2</sub> nanocomposites have been extensively studied in particular for their radiative short lifetime and enhanced emission efficiencies. In the present study, manganese doped ZnS-SiO<sub>2</sub> nanocomposites were also prepared and characterized.



*Chapter 2*

*Experimental Techniques*

## **CHAPTER 2 (EXPERIMENTAL METHODS)**

### **2.1 Materials**

ZnS-SiO<sub>2</sub> nanocomposites with different SiO<sub>2</sub> content and Mn doped ZnS-SiO<sub>2</sub> nanocomposites with different Zn<sup>2+</sup>:Mn<sup>2+</sup> mole ratios were synthesized by sol-gel method using the following chemicals; tetraethyl orthosilicate, ethanol, toluene, ammonia solution (25%), zinc acetate, manganese acetate and thioacetamide. All the chemicals used were of analytical grade and used without any further purification. All the experiments were carried out using Millipore water.

### **2.2 Equipment**

The various instrumental techniques that have been used for the characterization have been discussed briefly below.

#### **2.2.1 X-ray diffractometer**

X-ray diffraction patterns were recorded on a Bruker X-8 X-ray diffractometer using Cu K $\alpha$  line (1.5418Å) of the X-ray source. The 2 $\theta$  range studied was from 10° to 75° and the scan speed was 2° per minute. X-rays having wavelength similar to that of the size of the atom can be used to probe crystalline structure at the atomic level. Each crystalline solid has its unique X-ray pattern which may be used as a fingerprint for its identification. XRD is extensively being used for the determination of the crystalline structure of nanocrystals. In a crystalline solid, the broadening of a peak in the diffraction pattern can be used to determine the size of the crystallites by applying Debye- Scherer equation [36].

$$t = 0.9 \lambda / \beta \cos \theta$$

Where  $t$  is the average crystallite size,  $\lambda$  is the wavelength,  $\beta$  is the line broadening at half the maximum intensity in radians, and  $\theta$  is the Bragg's angle. The Scherrer equation is limited to nanoscale particles and it is not applicable to grains larger than about 0.1  $\mu\text{m}$ .

### ***2.2.2 Infrared Spectroscopy***

Infrared spectroscopy (IR spectroscopy) is the spectroscopy which deals with the infrared region of the electromagnetic spectrum. As with all spectroscopic techniques, it can be used to identify and study chemicals and organic bondings.

In the present study, IR spectra were obtained on a Thermo Nicolet NEXUS FT-IR spectrometer in mid IR range (from  $4000 \text{ cm}^{-1}$  to  $400 \text{ cm}^{-1}$ ) in KBr medium. All the spectra were recorded in the transmission mode.

### ***2.2.3 Field emission scanning electron microscope (FESEM) coupled with energy dispersive X-ray analysis (EDXA)***

An electron microscope is employed to produce an electronically magnified image of a specimen for finding its morphology. In an electron microscope, a beam of electrons illuminates the specimen and creates its magnified image. Unlike optical microscope, electron microscope can achieve magnifications up to 1,000,000 times or more because the wavelength is about 100,000 times shorter compared to the visible light radiation; optical microscopes are limited to 2000 times magnification.

SEM utilizes vacuum conditions and uses electrons to form an image that's why special preparations were made prior to the analysis of the samples. The metals, which are conductive, require no preparation before being used. All non-metals need to be made conductive by covering the sample with a thin layer of conductive material. This is done by using a device called a "sputter coater."

Since SEM relies on the surface process rather than transmission, it is able to image bulk samples up to many centimetres in size and has a great depth of field, and so can produce images that are good representations of the three-dimensional shape of samples [37].

In the present study, the surface morphology of the samples were analysed by FEI QUANTA-200F field emission scanning electron microscope having an accelerating voltage of 30 kV. The elemental analysis of the synthesized materials was performed using an EDXA accessory equipped with a CCD (charge coupled device) camera.

#### ***2.2.4 Diffuse reflectance spectroscopy***

Diffuse reflection is a process whereby light reflected from an object strikes other objects in the surrounding area, illuminating them. Diffuse reflection specifically describes light reflected from objects which are not shiny or specular.

Diffuse reflectance is an excellent sampling tool for powdered materials in the mid-IR, near infrared and visible ranges. It can also be used for the analysis of intractable solid samples. In the present study, a Shimadzu UV-3600 UV-Vis NIR spectrometer was used and the range studied was from 200 to 800 nm. The samples to be analysed by diffuse reflectance were mixed with barium sulphate (1:100 wt. ratio) prior to the analysis.

### ***2.2.5 Fluorescence spectroscopy***

Fluorescence spectroscopy is a type of electromagnetic spectroscopy which analyzes fluorescence from a sample. It involves using a beam of light, usually ultraviolet light, that excites the electrons in molecules of certain compounds and causes them to emit light of a lower energy.

A fluorimeter is a device used to measure parameters of the fluorescence, i.e. intensity and wavelength distribution of emission spectrum after excitation [38]. These parameters are used to identify the presence and the amount of specific molecules in a specimen. Fluorescence analysis can be orders of magnitude more sensitive than other techniques. Applications include chemistry/biochemistry, medicine, environmental monitoring, etc. Generally fluorescent compounds have two characteristic spectra: an excitation spectrum (the wavelength and the amount of light absorbed) and an emission spectrum (the wavelength and the amount of light emitted). No two compounds have the same fluorescence signature. It is this principle that makes fluorescence spectroscopy a highly specific analytical technique.

In the present study, the measurements were carried on a Shimadzu RF-5301 PC spectrometer with an excitation wavelength 315 nm. The emission spectra were recorded from 325 to 800 nm. The samples were prepared by adding 10mg each of the powder samples to 5ml ethanol followed by sonication prior to the analysis.

### ***2.2.6 Thermal gravimetric analysis***

Thermal gravimetric analysis (TGA) is a type of testing performed on samples that determines changes in weight percentage in relation to change in temperature [39]. A derivative weight loss curve can identify the point where the weight loss is most apparent. TGA is commonly employed

in research and testing to determine degradation temperatures, absorbed moisture content of materials and the level of inorganic and organic components in materials. In the present study, the TGA patterns of the samples were recorded using a Perkin Elmer (Pyris Diamond) instrument from room temperature to 900°C in the presence of nitrogen gas with a heating rate of 10°C per minute.

### ***2.3 Methodology***

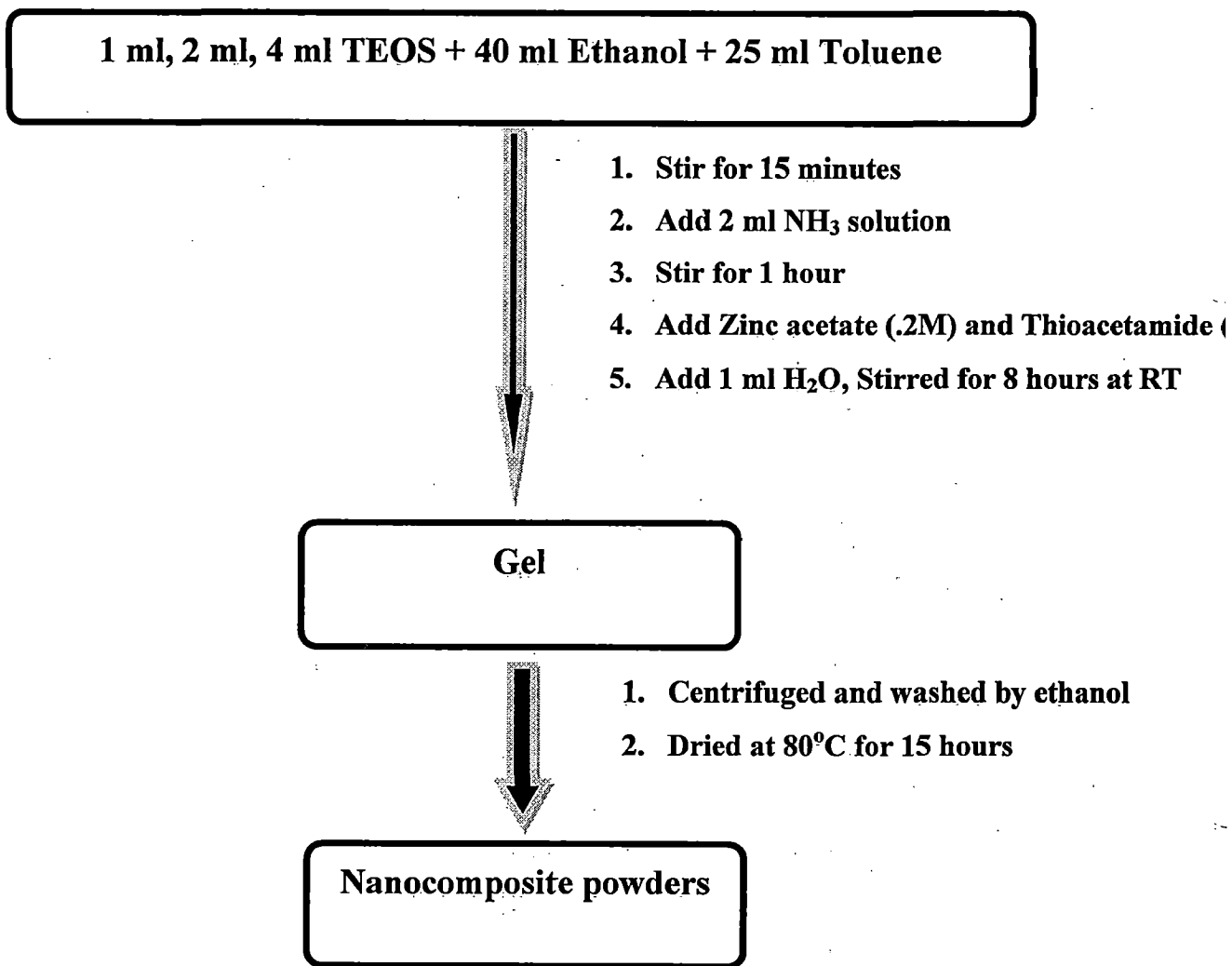
ZnS-SiO<sub>2</sub> nanocomposites have been synthesized in the literature by the following methods.

- Micro emulsion [40]
- RF sputtering [41]
- Sol gel process [42,43]
- Wet chemical route [44]

In the present study, ZnS-SiO<sub>2</sub> nanocomposites with different SiO<sub>2</sub> ratios (Scheme-1) and Mn doped ZnS-SiO<sub>2</sub> nanocomposites (Scheme-2) with different Zn<sup>2+</sup>:Mn<sup>2+</sup> mole ratios were synthesized by the sol-gel method.

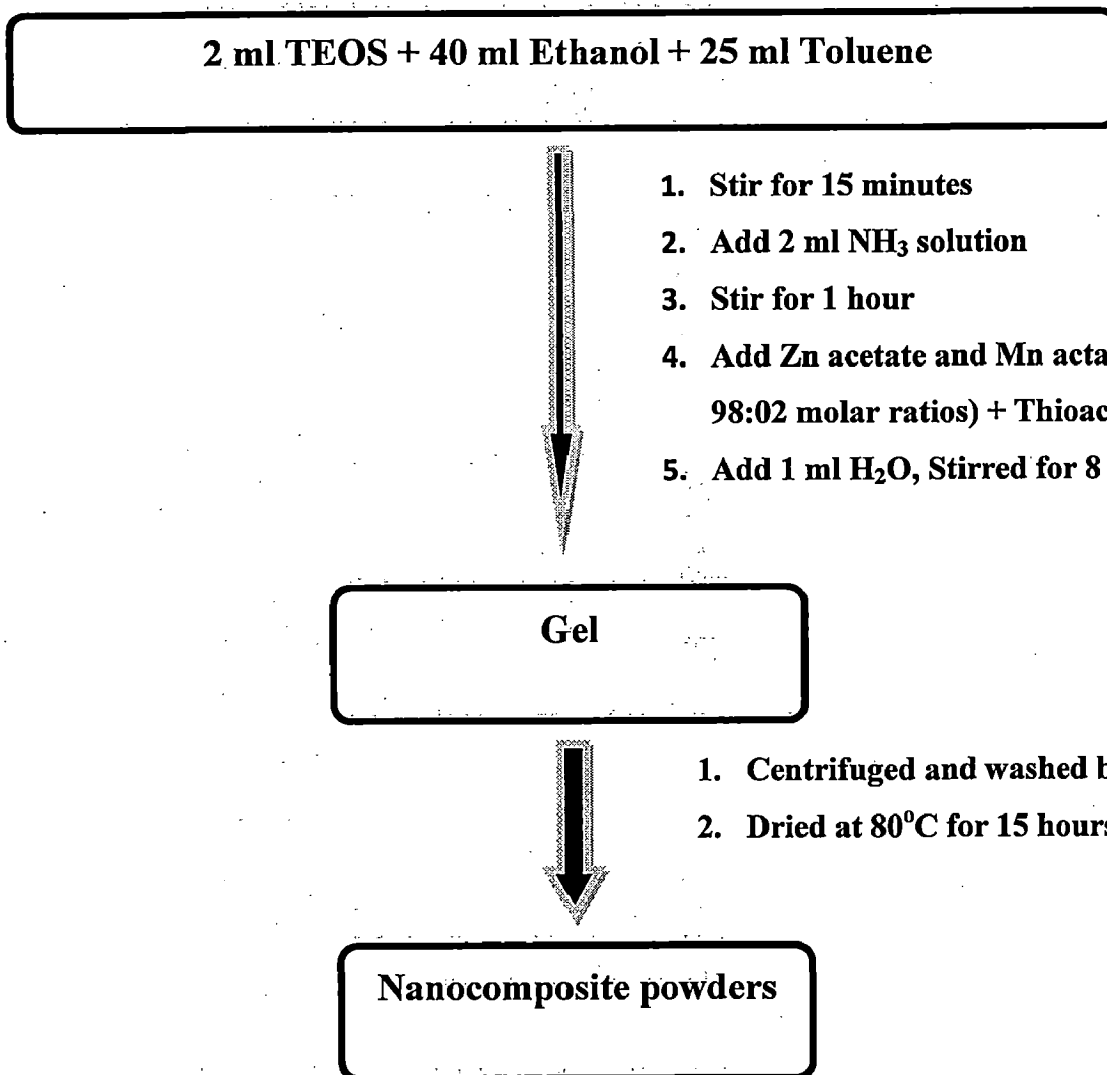
For the synthesis of ZnS-SiO<sub>2</sub> nanocomposites, zinc acetate and thioacetamide were taken in a 1:1 molar ratio and then a mixture of 40 ml ethanol, 25 ml toluene and tetraethyl orthosilicate (1ml, 2ml, 4ml) were added. This was followed by the addition of ammonia solution (2 ml) along with a small amount of distilled water (1 ml). The contents were stirred at room temperature for 8 hours. The gel obtained was dried at 80°C for 15 hours [44, 45].

Mn doped ZnS-SiO<sub>2</sub> nanocomposites with variable Zn<sup>2+</sup>:Mn<sup>2+</sup> mole ratios (98:02, 95:05, 90:10) were also synthesized by the above procedure by introducing manganese acetate during the synthesis while keeping all the other conditions same (see Scheme-2).



Scheme-1: Synthetic procedure for ZnS-SiO<sub>2</sub> nanocomposites with variable SiO<sub>2</sub> ratios.





Scheme-2: Synthetic procedure for Mn doped ZnS-SiO<sub>2</sub> nanocomposites with variable Zn<sup>2+</sup>:Mn<sup>2+</sup> molar ratios.

The nomenclature of different ZnS-SiO<sub>2</sub> nanocomposites prepared in the present study are given below.

Sample **a** = Pure ZnS

ZnS-SiO<sub>2</sub>-1 = ZnS-SiO<sub>2</sub> nanocomposite prepared with 1 ml TEOS

ZnS-SiO<sub>2</sub>-2 = ZnS-SiO<sub>2</sub> nanocomposite prepared with 2 ml TEOS

ZnS-SiO<sub>2</sub>-3 = ZnS-SiO<sub>2</sub> nanocomposite prepared with 4 ml TEOS

Sample **a1** = Mn doped ZnS-SiO<sub>2</sub> nanocomposite prepared with Zn<sup>2+</sup>: Mn<sup>2+</sup> = 98:02 mole ratio

Sample **a2** = Mn doped ZnS-SiO<sub>2</sub> nanocomposite prepared with Zn<sup>2+</sup>: Mn<sup>2+</sup> = 95:05 mole ratio

Sample **a3** = Mn doped ZnS-SiO<sub>2</sub> nanocomposite prepared with Zn<sup>2+</sup>: Mn<sup>2+</sup> = 90:10 mole ratio



*Chapter 3*

*Results and Discussion*

*ZnS-SiO<sub>2</sub> Nanocomposites*

## CHAPTER 3 RESULTS AND DISCUSSION

### ***ZnS-SiO<sub>2</sub> NANOCOMPOSITES:***

#### ***3.1 XRD analysis of ZnS-SiO<sub>2</sub> nanocomposites***

Fig. 3.1.1 shows the XRD patterns of ZnS-SiO<sub>2</sub> nanocomposites with variable SiO<sub>2</sub> ratios, i.e. ZnS-SiO<sub>2</sub>-1, ZnS-SiO<sub>2</sub>-2 and ZnS-SiO<sub>2</sub>-3. There are three diffraction peaks which correspond to (111), (220), (311) planes of cubic crystalline ZnS [36] and the patterns matched well with the standard JCPDS data (File no 05-0566). The crystallite size of pure ZnS was calculated using Debye-Scherrer equation and it was around 2.2 nm whereas the crystallite size of ZnS-SiO<sub>2</sub> nanocomposites were calculated to be about 1.8 nm. It is concluded that the crystallite size of ZnS in ZnS-SiO<sub>2</sub> nanocomposites is decreased in comparison with pure ZnS.

Fig 3.1.2 shows the XRD patterns of ZnS-SiO<sub>2</sub> nanocomposites with variable SiO<sub>2</sub> ratios calcined at 400°C. The calculated crystallite size of ZnS in ZnS-SiO<sub>2</sub> nanocomposites with variable SiO<sub>2</sub> ratios calcined at 400°C, were 4.2 nm, 4.7 nm and 5.1 nm for ZnS-SiO<sub>2</sub>-1, ZnS-SiO<sub>2</sub>-2 and ZnS-SiO<sub>2</sub>-3, respectively in comparison to 1.8 nm of the as prepared nanocomposites.

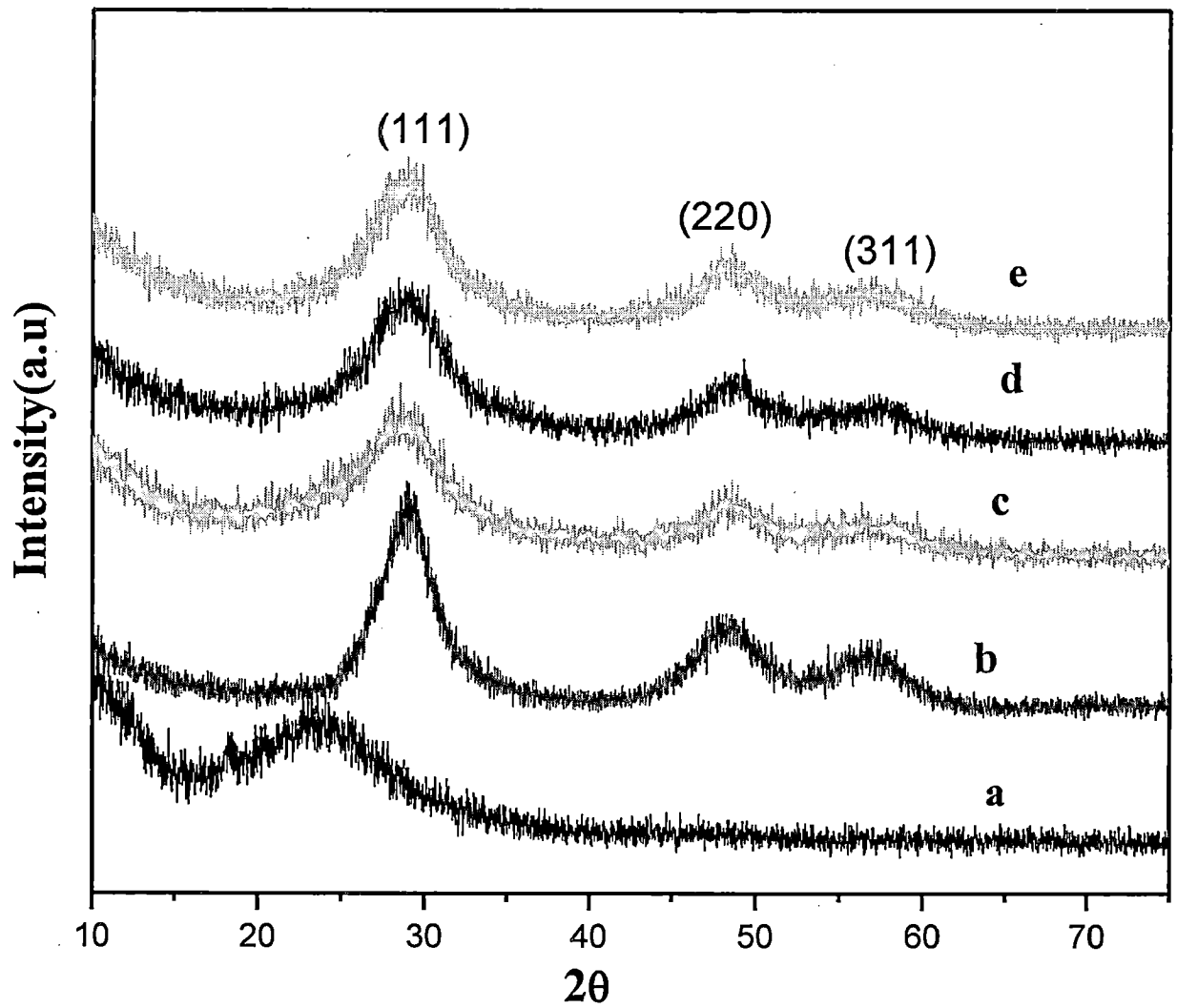


Fig.3.1.1 XRD patterns of (a)  $\text{SiO}_2$ , (b)  $\text{ZnS}$ , (c)  $\text{ZnS-SiO}_2-1$ , (d)  $\text{ZnS-SiO}_2-2$  and (e)  $\text{ZnS-SiO}_2-3$ .

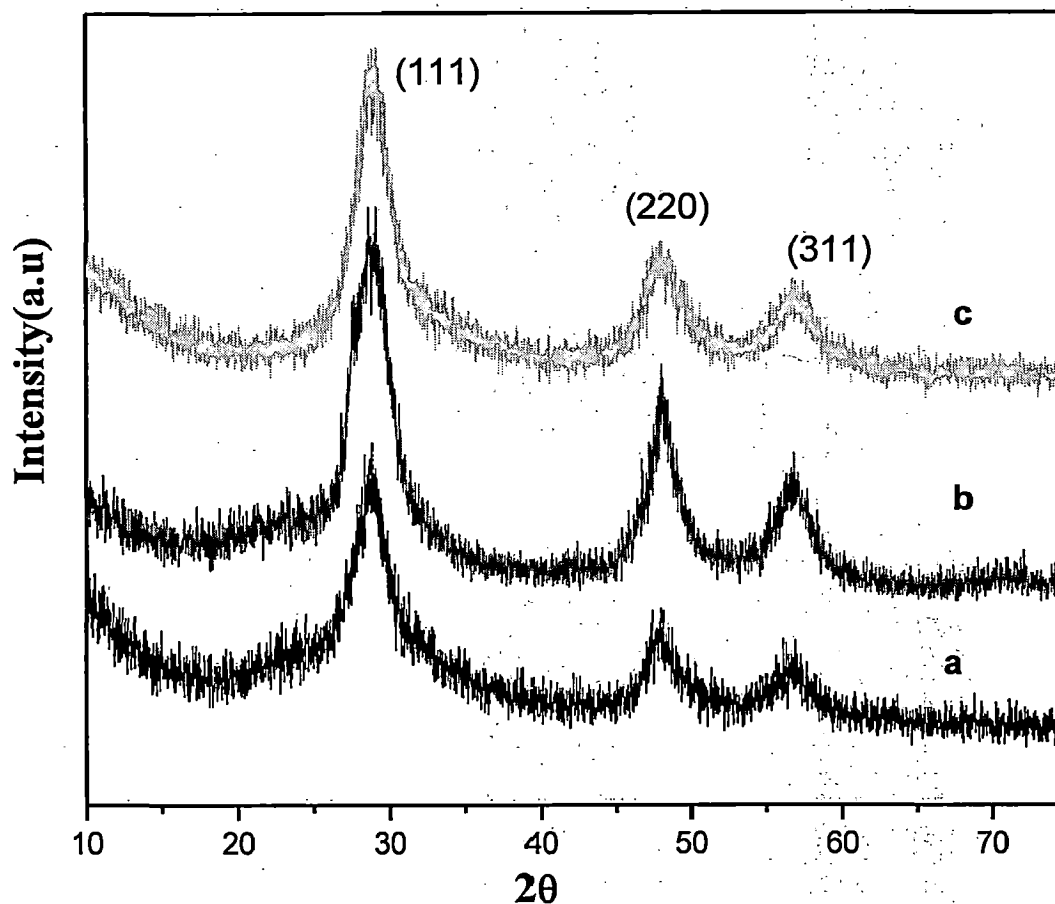


Fig. 3.1.2 XRD patterns of (a) ZnS-SiO<sub>2</sub>-1, (b) ZnS-SiO<sub>2</sub>-2 and (c) ZnS-SiO<sub>2</sub>-3 nanocomposites calcined at 400°C.

### 3.2 FE-SEM images and EDXA analysis of ZnS-SiO<sub>2</sub> nanocomposites:

Fig. 3.2.1 shows the FE-SEM images of pure ZnS, ZnS-SiO<sub>2</sub> nanocomposites prepared with different SiO<sub>2</sub> ratios, i.e. ZnS-SiO<sub>2</sub>-1, ZnS-SiO<sub>2</sub>-2 and ZnS-SiO<sub>2</sub>-3 and pure SiO<sub>2</sub>. The images show that the nanoparticles in the composites are spherical in shape and are agglomerated but in the case of pure SiO<sub>2</sub>, the nanoparticles are spherical shape, regular and distinct. From the images it was concluded that the particle size is decreased from 2.2 nm to 1.8 nm in ZnS-SiO<sub>2</sub> nanocomposites in comparison to pure ZnS nanoparticles. Fig. 3.2.2 shows the FE-SEM images of ZnS-SiO<sub>2</sub> nanocomposites prepared with different SiO<sub>2</sub> ratios, i.e. ZnS-SiO<sub>2</sub>-1, ZnS-SiO<sub>2</sub>-2

and ZnS-SiO<sub>2</sub>-3 after calcination at 400°C. The morphology of annealed samples is approximately same as that of as prepared samples but with increased particle size.

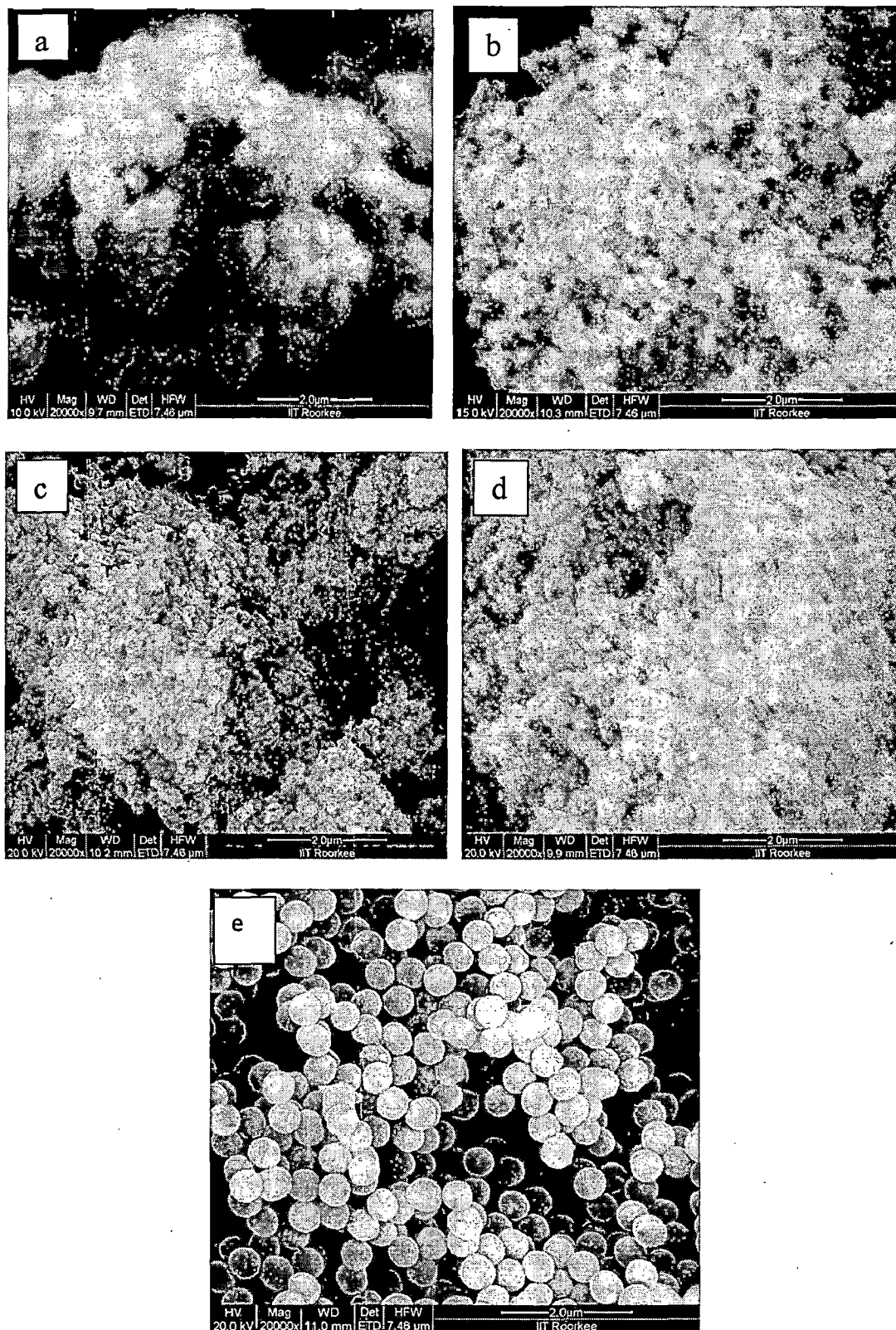


Fig.3.2.1 FE-SEM images of (a) pure ZnS, (b) ZnS-SiO<sub>2</sub>-1, (c) ZnS-SiO<sub>2</sub>-2, (d) ZnS-SiO<sub>2</sub>-3 and (e) pure SiO<sub>2</sub>

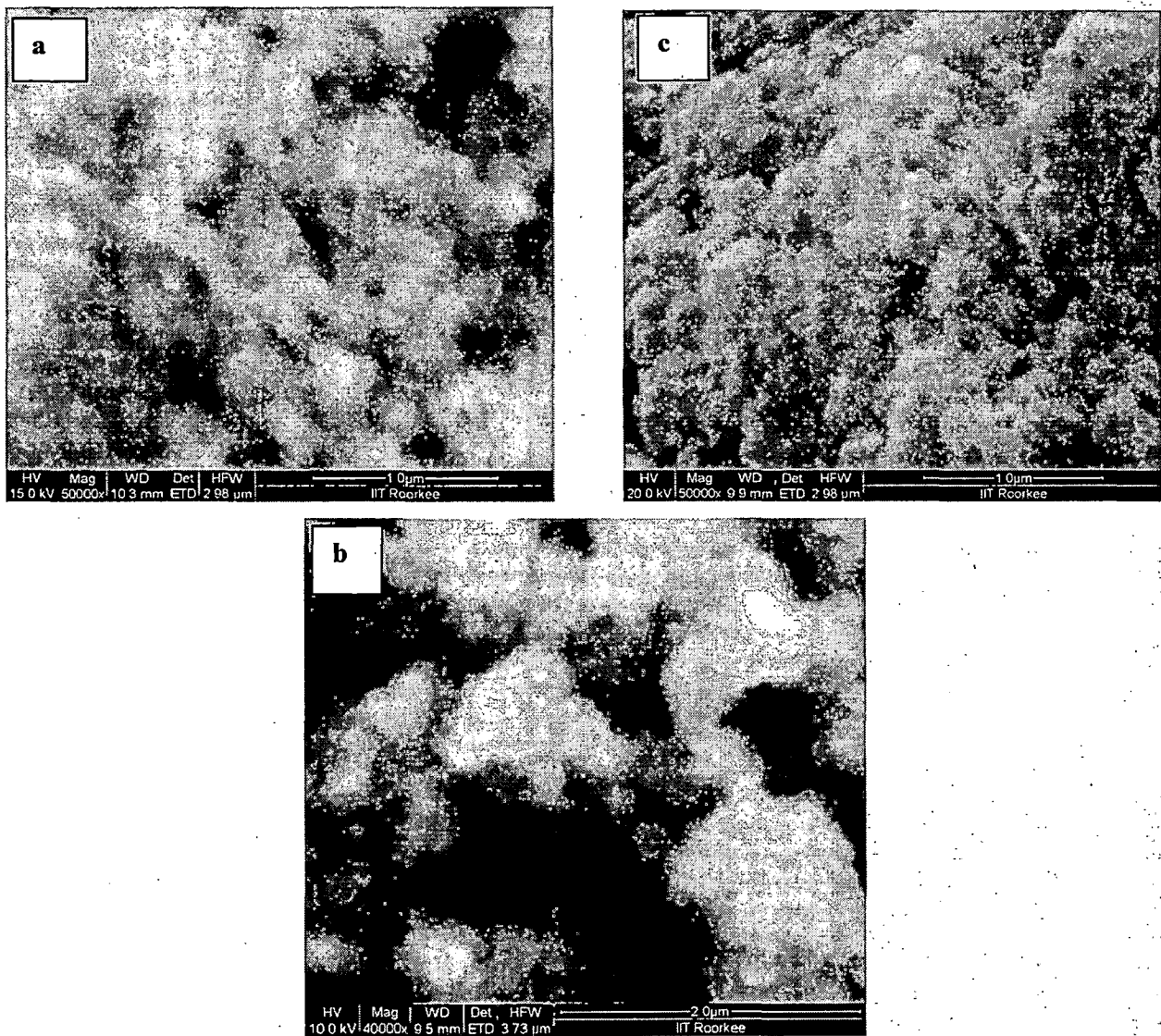
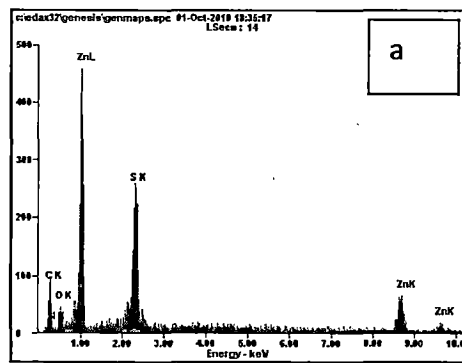
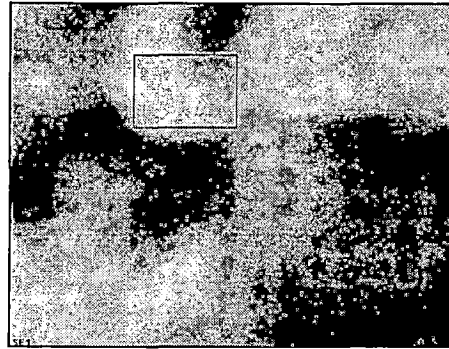


Fig.3.2.2 FE-SEM images of (a) ZnS-SiO<sub>2</sub>-1, (b) ZnS-SiO<sub>2</sub>-2 and (c) ZnS-SiO<sub>2</sub>-3 calcined at 400°C

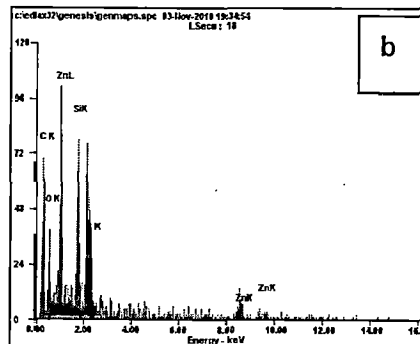
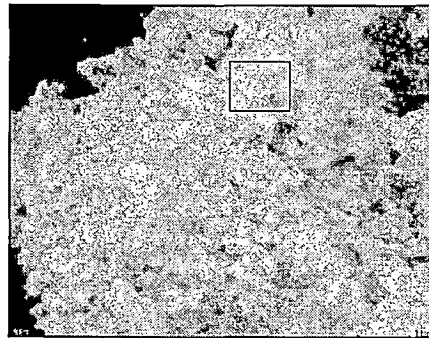
Fig. 3.2.3 shows the EDXA data for pure ZnS nanoparticles, ZnS-SiO<sub>2</sub>-1, ZnS-SiO<sub>2</sub>-2, ZnS-SiO<sub>2</sub>-3 nanocomposites and pure SiO<sub>2</sub> nanoparticles. The EDXA patterns of different ZnS-SiO<sub>2</sub> nanocomposites with variable SiO<sub>2</sub> ratios confirm the presence of Zn, S, Si and O elements with different weight percentages.



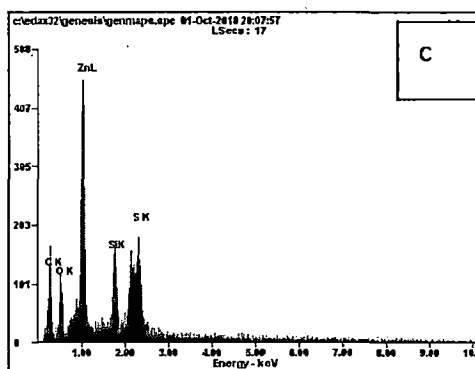
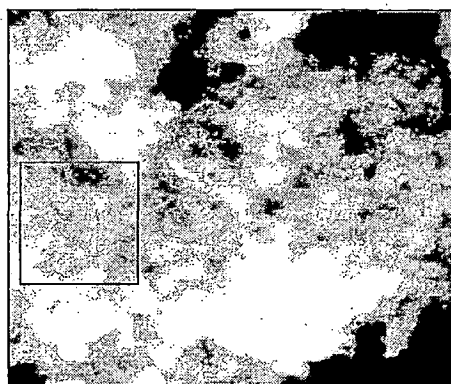
Element	Wt%	At%
<i>CK</i>	26.73	60.17
<i>NK</i>	00.00	00.00
<i>OK</i>	02.73	04.61
<i>SK</i>	14.05	11.85
<i>ZnK</i>	56.49	23.36
<b>Matrix</b>	Correction	ZAF



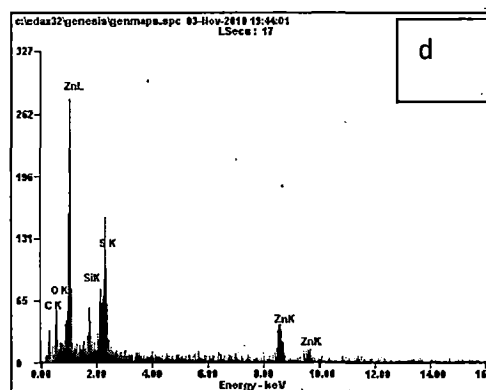
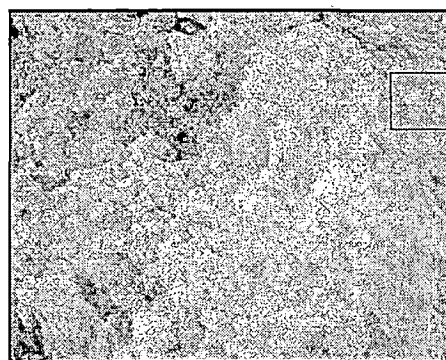
Element	Wt%	At%
<i>CK</i>	49.70	72.84
<i>OK</i>	10.74	11.81
<i>SiK</i>	08.79	05.51
<i>SK</i>	05.56	03.05
<i>ZnK</i>	25.22	06.79
<b>Matrix</b>	Correction	ZAF



Element	Wt%	At%
CK	33.25	60.98
OK	07.32	10.08
ZnL	36.33	12.24
SiK	08.63	06.77
SK	14.46	09.93
Matrix	Correction	ZAF



Element	Wt%	At%
CK	38.22	63.07
OK	13.73	17.01
SiK	04.04	02.85
SK	11.84	07.32
ZnK	32.17	09.75
Matrix	Correction	ZAF



<i>Element</i>	<i>Wt%</i>	<i>At%</i>
<i>CK</i>	06.48	10.72
<i>NK</i>	03.42	04.86
<i>OK</i>	38.75	48.11
<i>SiK</i>	51.35	36.32
<i>Matrix</i>	Correction	ZAF

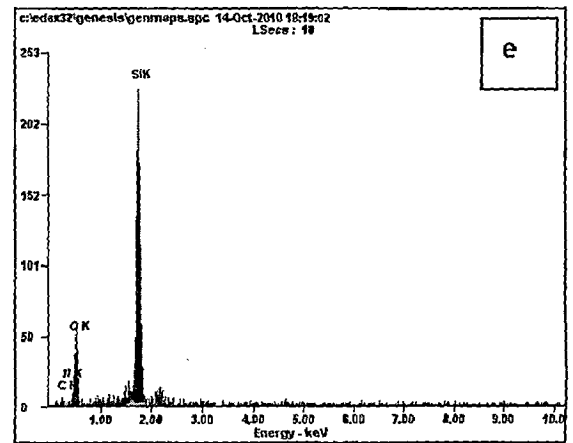
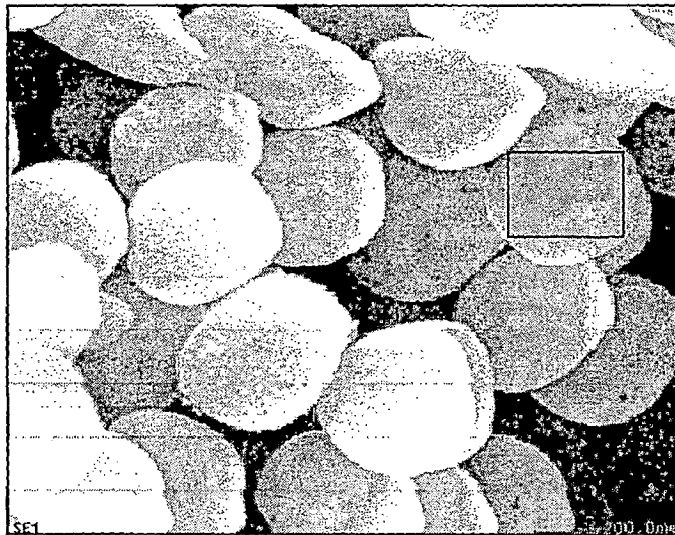


Fig. 3.2.3 EDXA data of (a) pure ZnS, (b) ZnS-SiO<sub>2</sub>-1, (c) ZnS-SiO<sub>2</sub>-2, (d) ZnS-SiO<sub>2</sub>-3 and (e) pure SiO<sub>2</sub>

### 3.3 FT-IR analysis of ZnS-SiO<sub>2</sub> nanocomposites:

Fig. 3.3.1 shows the FT-IR spectrum of pure SiO<sub>2</sub>. The band around 1081 cm<sup>-1</sup> is due to Si-O-Si asymmetric stretching whereas the band at about 795 cm<sup>-1</sup> is due to Si-O-Si symmetric stretching. The band around 464 cm<sup>-1</sup> is due to Si-O-Si bending [46]. The bands around 3448 cm<sup>-1</sup> and 1642 cm<sup>-1</sup> are due to O-H stretching and OH bending, respectively.

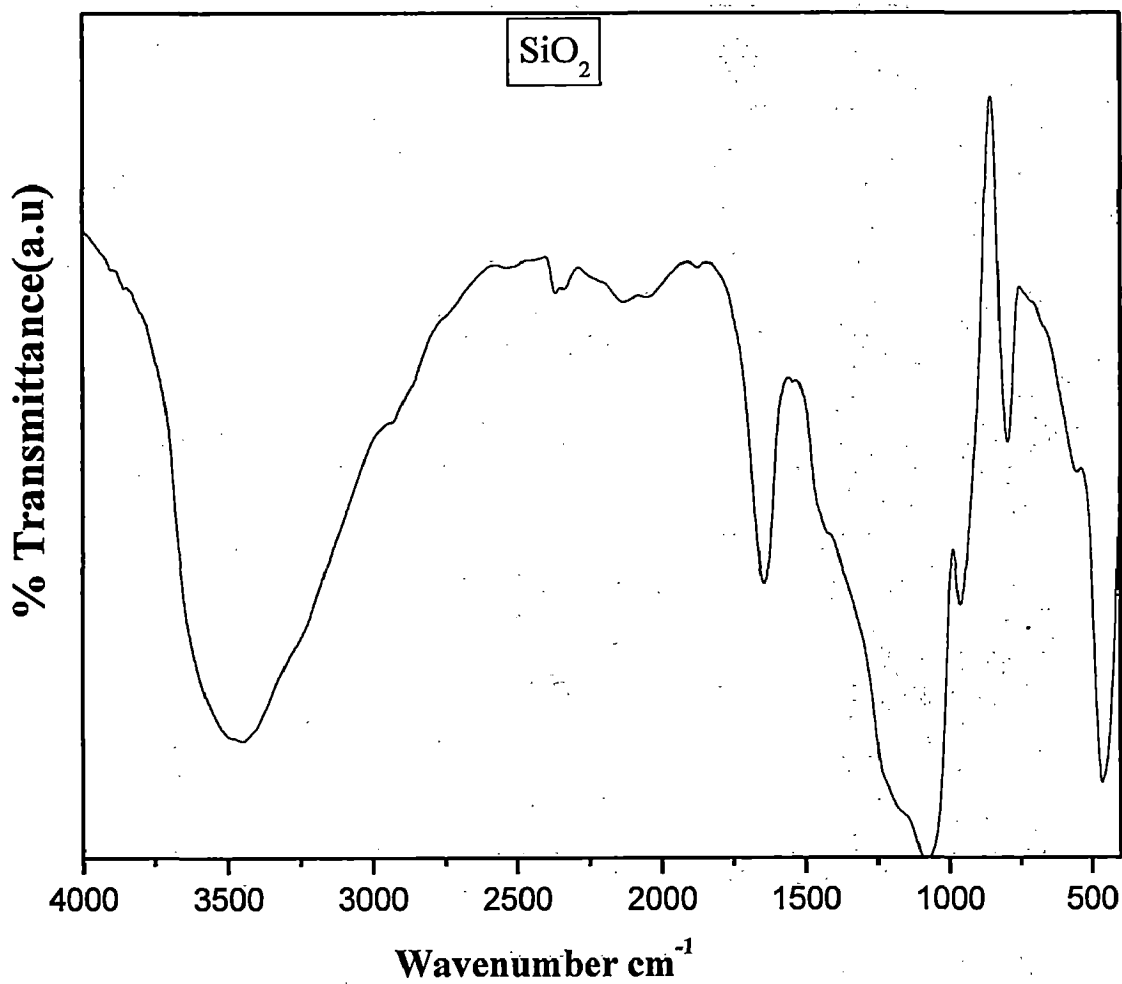


Fig. 3.3.1 FTIR spectrum of pure SiO<sub>2</sub>.

Fig. 3.3.2 shows the FT-IR spectra of pure ZnS and ZnS-SiO<sub>2</sub> nanocomposites with different SiO<sub>2</sub> ratios. In the spectra, the band around 1065 cm<sup>-1</sup> is due to Si-O-Si asymmetric stretching where as the band at about 791 cm<sup>-1</sup> is due to Si-O-Si symmetric stretching. The band at 460 cm<sup>-1</sup> is due to Si-O-Si bending [46, 47]. The band at 619 cm<sup>-1</sup> is assigned to Zn-S stretching. In the case of ZnS-SiO<sub>2</sub> nanocomposites, the band around 3330cm<sup>-1</sup> is due to O-H stretching and the band around 1402 cm<sup>-1</sup> is due to OH bending [48].

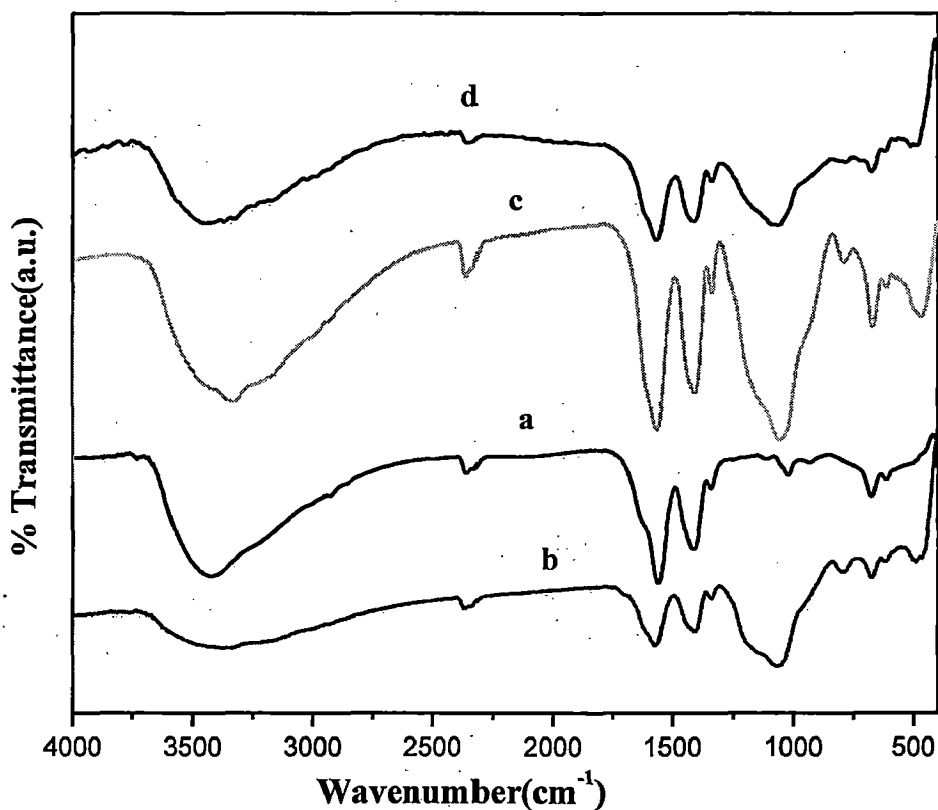


Fig. 3.3.2 FTIR spectra of (a) pure ZnS, (b) ZnS-SiO<sub>2</sub>-1, (c) ZnS-SiO<sub>2</sub>-2, and (d) ZnS-SiO<sub>2</sub>-3.

### 3.4 Thermal gravimetric analysis of ZnS nanoparticles and ZnS-SiO<sub>2</sub> nanocomposites

Fig. 3.4.1 shows the TGA pattern of pure ZnS, ZnS-SiO<sub>2</sub>-1, ZnS-SiO<sub>2</sub>-2 and ZnS-SiO<sub>2</sub>-3 nanocomposites. The thermal decomposition behaviour of the nanocomposites is similar to that of pure ZnS nanoparticles.

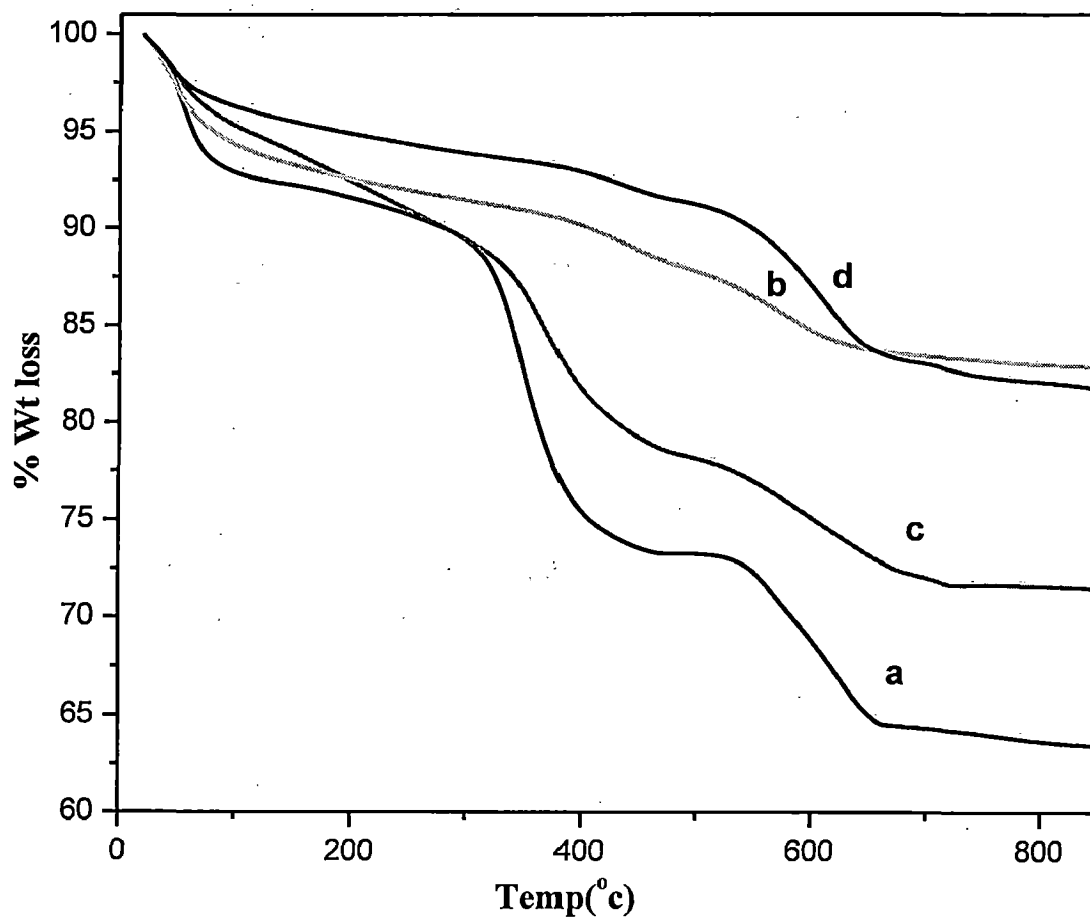


Fig. 3.4.1 TGA data of (a) pure ZnS, (b) ZnS-SiO<sub>2</sub>-1, (c) ZnS-SiO<sub>2</sub>-2 and (d) ZnS-SiO<sub>2</sub>-3.

### ***3.5 Diffuse reflectance spectral analysis of ZnS-SiO<sub>2</sub> nanocomposites:***

Fig. 3.5.1 shows the diffuse reflectance spectra of pure ZnS and ZnS-SiO<sub>2</sub> nanocomposites with different SiO<sub>2</sub> ratios, i.e. ZnS-SiO<sub>2</sub>-1, ZnS-SiO<sub>2</sub>-2 and ZnS-SiO<sub>2</sub>-3. The bandgap of ZnS nanoparticles was estimated as 4.9 eV which is greater than the bandgap of ZnS-SiO<sub>2</sub>-2 (4.4eV) (Fig. 3.5.2). In the other two ZnS-SiO<sub>2</sub> nanocomposites (ZnS-SiO<sub>2</sub>-1 and ZnS-SiO<sub>2</sub>-3), the bandgap were calculated to be around 5.1eV and 5.2eV. When the concentration of TEOS was increased twice or decreased by half during the synthesis of nanocomposites, the bandgap of ZnS-SiO<sub>2</sub> nanocomposites is increased from 4.4eV to 5.2eV. The band gap of bulk ZnS is 3.7 eV [49].

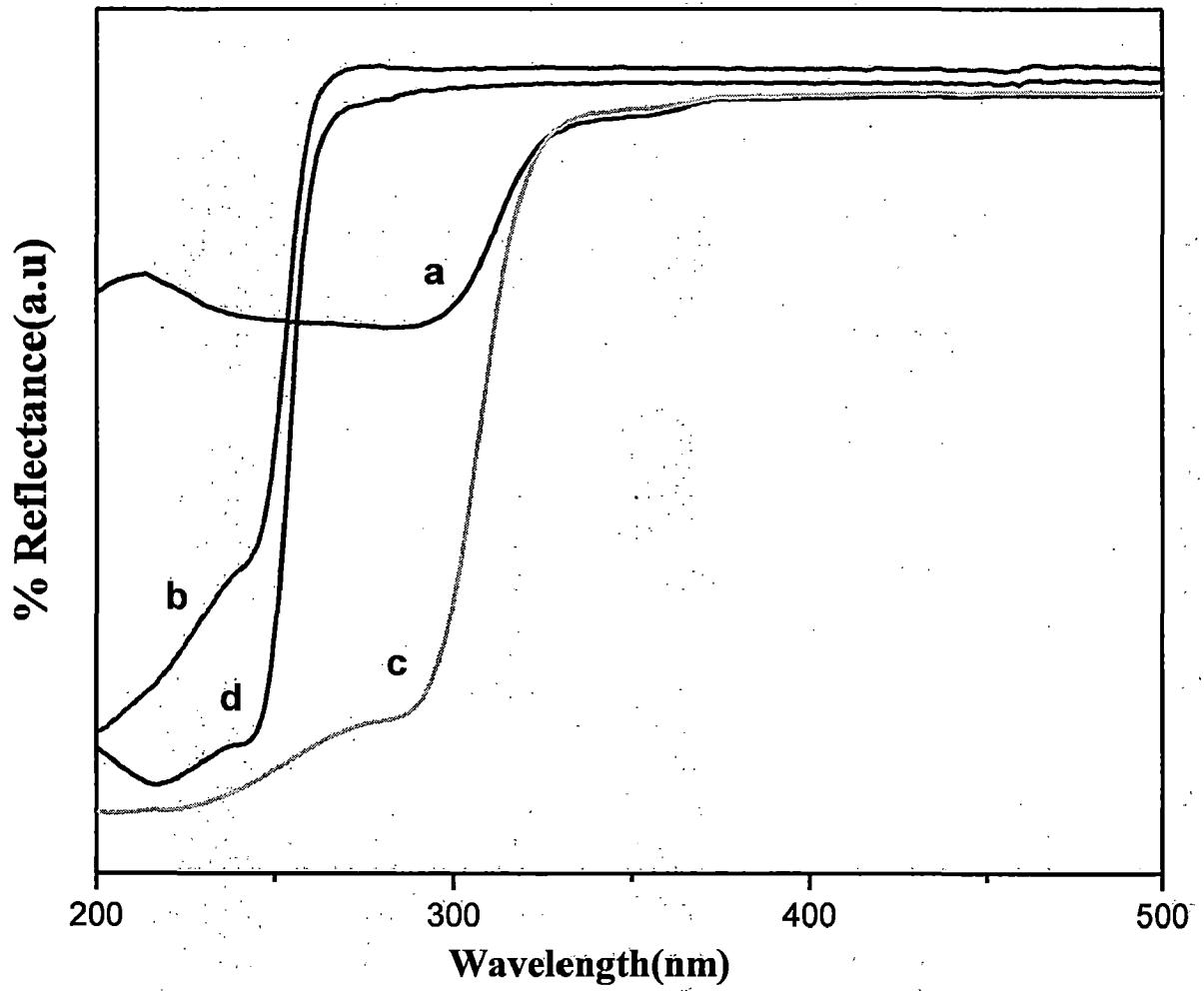


Fig. 3.5.1 DRS spectra of (a) pure ZnS, (b) ZnS-SiO<sub>2</sub>-1, (c) ZnS-SiO<sub>2</sub>-2 and (d) ZnS-SiO<sub>2</sub>-3.



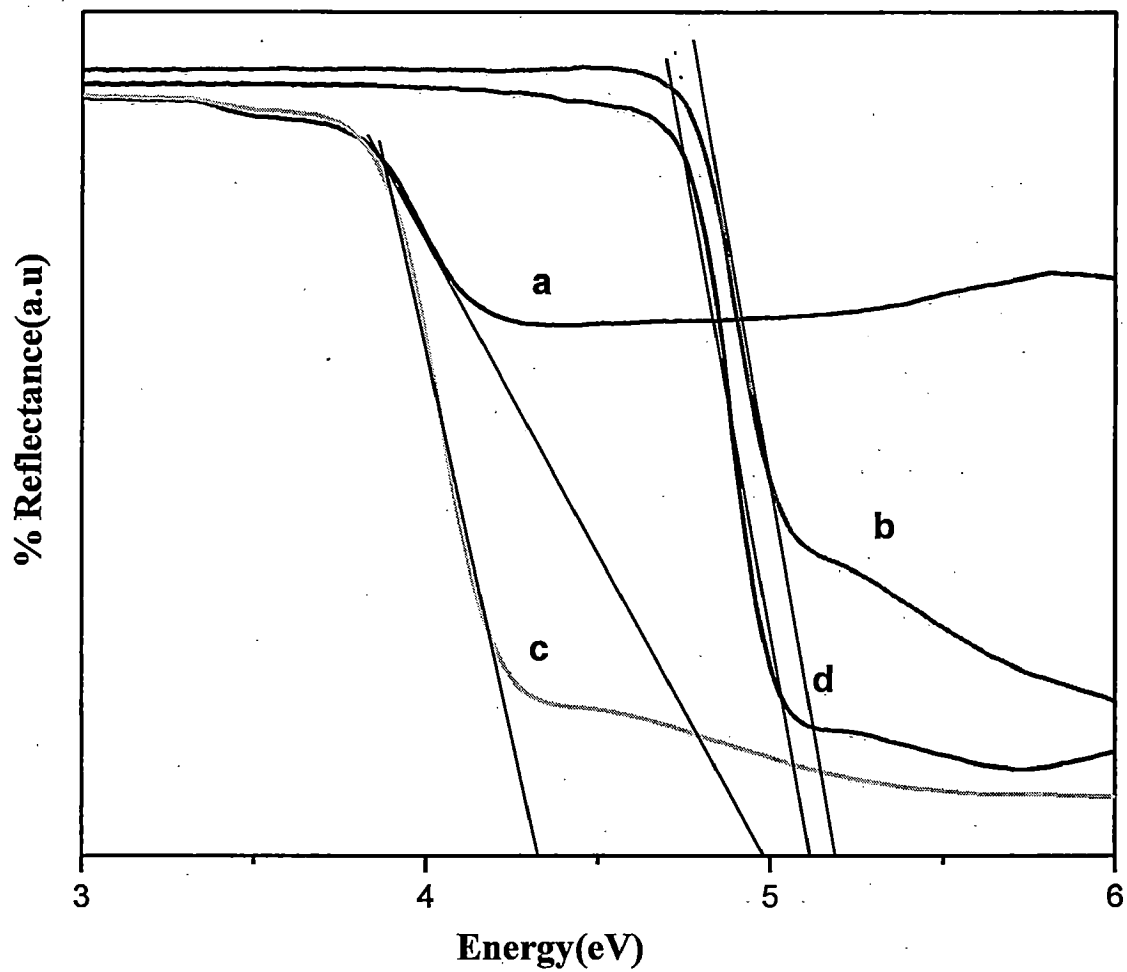


Fig. 3.5.2 DRS spectra of (a) pure ZnS, (b) ZnS-SiO<sub>2</sub>-1, (c) ZnS-SiO<sub>2</sub>-2 and (d) ZnS-SiO<sub>2</sub>-3

### 3.6 Photoluminescence spectra of ZnS nanoparticles and ZnS-SiO<sub>2</sub> nanocomposites:

Fig. 3.6.1 shows the photoluminescence spectra of pure ZnS nanoparticles and ZnS-SiO<sub>2</sub> nanocomposites with different SiO<sub>2</sub> ratios, i.e. ZnS-SiO<sub>2</sub>-1, ZnS-SiO<sub>2</sub>-2 and ZnS-SiO<sub>2</sub>-3. The photoluminescence spectra were recorded with an excitation wavelength of 325 nm at room temperature. The emission spectra show the maximum intensity at 421nm in sample d (ZnS-SiO<sub>2</sub>-3) caused by sulphur vacancies. In sample a (pure ZnS), the peak around 389 nm is attributed to zinc vacancies [50].

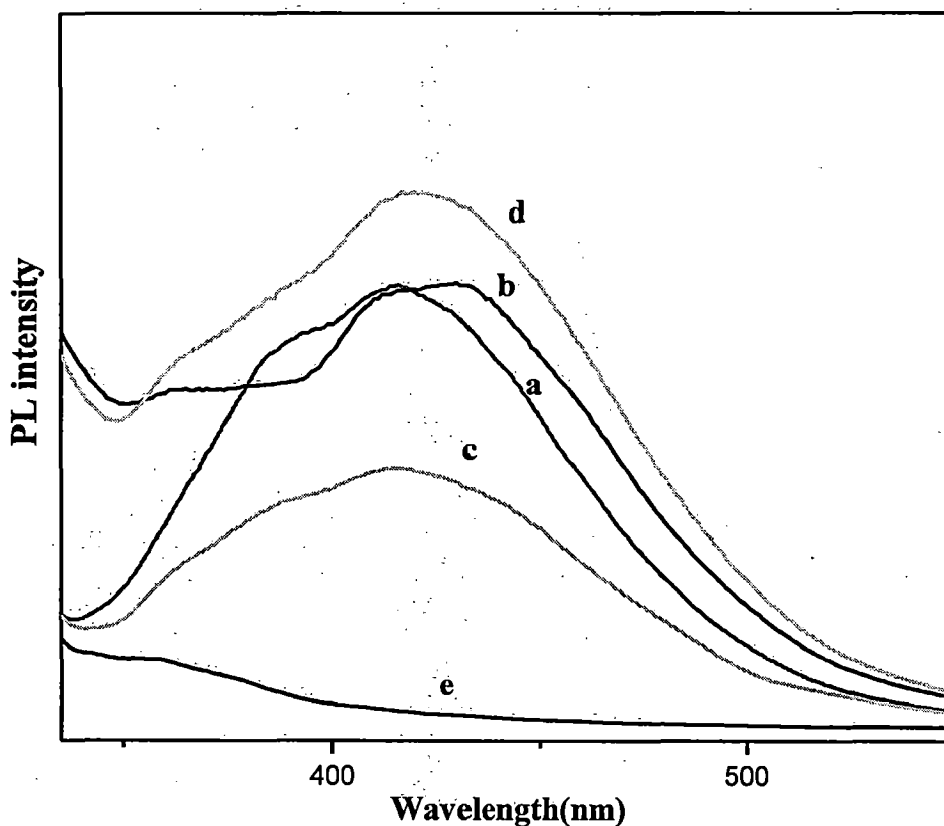


Fig.3.6.1 PL spectra of (a) pure ZnS, (b) ZnS-SiO<sub>2</sub>-1, (c) ZnS-SiO<sub>2</sub>-2, (d) ZnS-SiO<sub>2</sub>-3 and (e) ethanol.

Fig. 3.6.2 shows the photoluminescence spectra of ZnS-SiO<sub>2</sub> nanocomposites with different SiO<sub>2</sub> ratios calcined at 400°C. In case of samples ZnS-SiO<sub>2</sub>-2 and ZnS-SiO<sub>2</sub>-3, the PL intensity decreased in comparison to the nanocomposites before calcination. In the case of sample ZnS-SiO<sub>2</sub>-1, the PL peak at about 464 nm is intense. The band around around 365 is due to the solvent (methanol). The band around 389 is due to zinc vacancies.

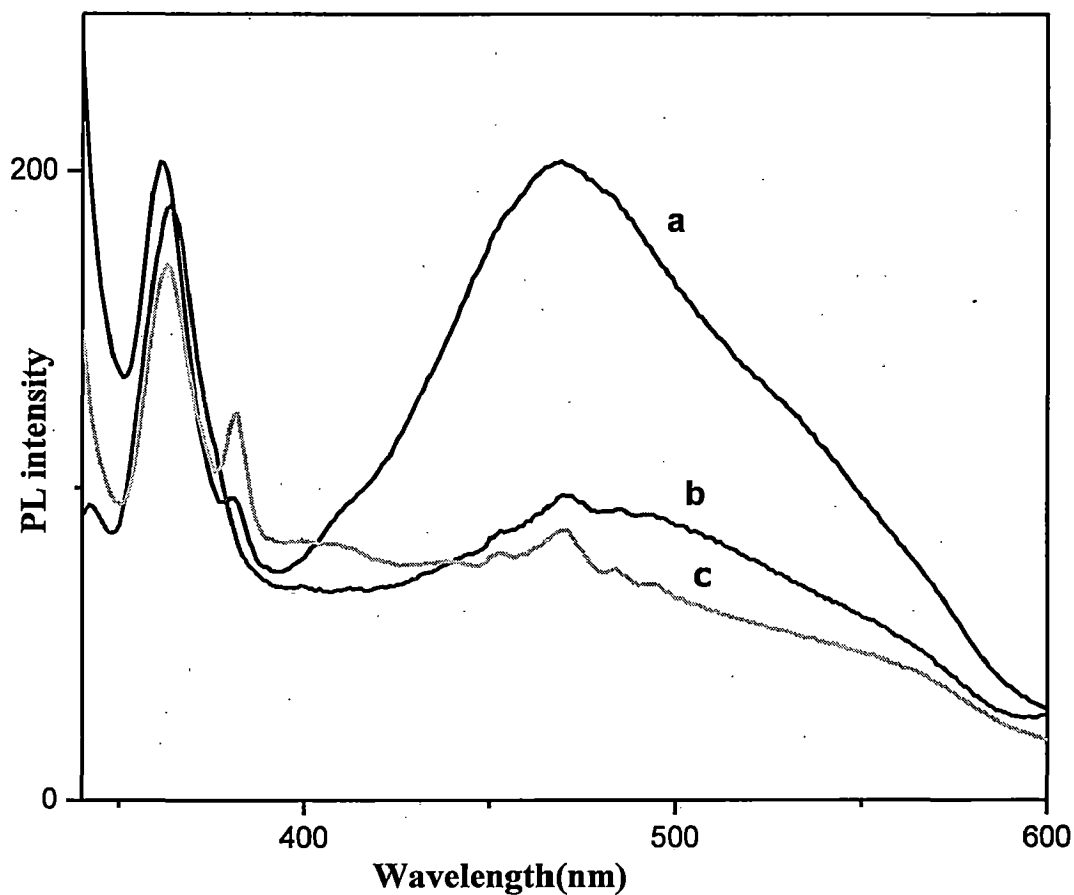


Fig. 3.6.2 PL spectra of (a) ZnS-SiO<sub>2</sub>-1, (b) ZnS-SiO<sub>2</sub>-2 and (c) ZnS-SiO<sub>2</sub>-3 after calcination at 400°C.



*Chapter 4*

*Mn doped ZnS-SiO<sub>2</sub>  
Nanocomposites*

## CHAPTER 4

### **Mn DOPED ZnS-SiO<sub>2</sub> NANOCOMPOSITES:**

#### ***4.1 XRD analysis of Mn doped ZnS-SiO<sub>2</sub> nanocomposites:***

Fig. 4.1.1 shows the XRD patterns of ZnS-SiO<sub>2</sub> nanocomposite ZnS-SiO<sub>2</sub>-2 and Mn doped ZnS-SiO<sub>2</sub> nanocomposites with variable Zn:Mn molar ratios. In the XRD patterns, there are three diffraction peaks corresponding to (111), (220), (311) reflections of cubic crystalline ZnS [35]. The crystallite size of Mn doped ZnS-SiO<sub>2</sub> nanocomposites with variable Zn:Mn in molar ratios was calculated as about 1.4 nm whereas the crystallite size of ZnS in ZnS-SiO<sub>2</sub>-2 nanocomposite was calculated as 1.8 nm.

Fig. 4.1.2 shows the XRD patterns of Mn doped ZnS-SiO<sub>2</sub> nanocomposites with variable Zn:Mn molar ratios after calcination at 400°C. The crystallite size of calcined samples increased to 2.9 nm as compared to 1.4 nm for the samples before calcination.

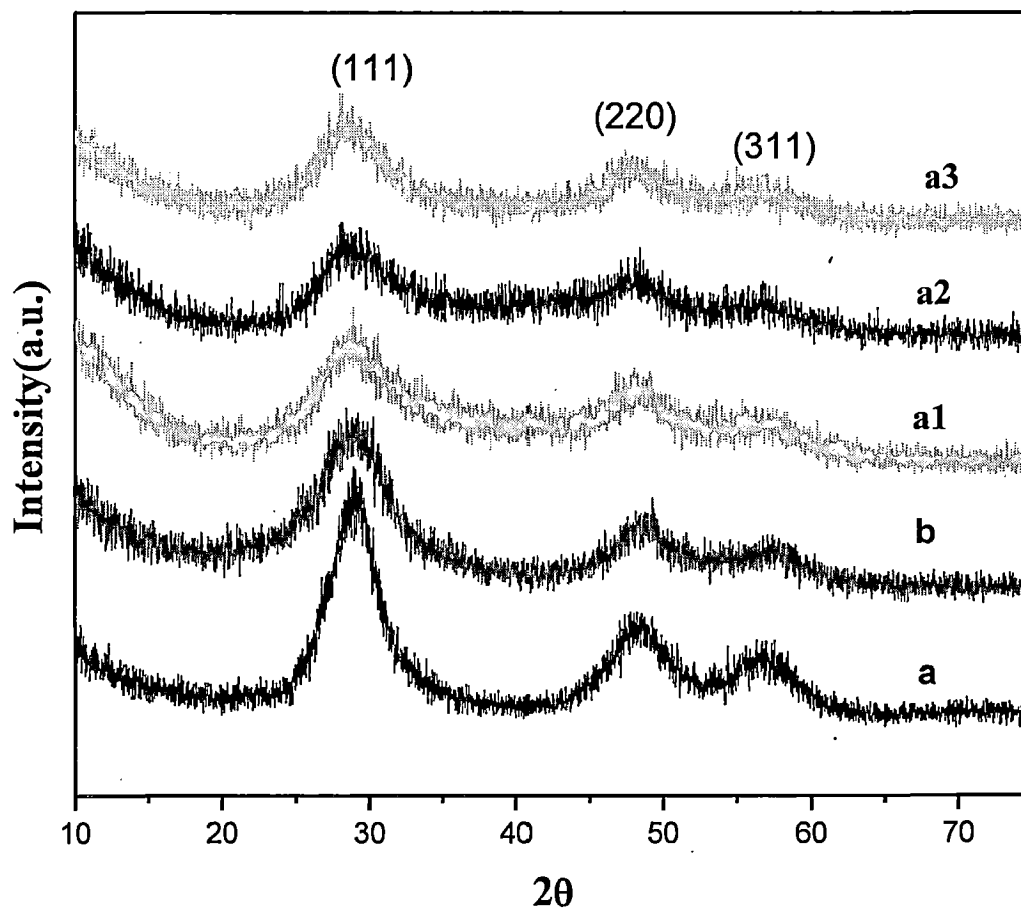


Fig. 4.1.1 XRD patterns of (a) pure ZnS, (b) ZnS-SiO<sub>2</sub>-2 and Mn doped ZnS-SiO<sub>2</sub> nanocomposites (a1, a2 and a3).

Where a1, a2, a3 are Mn doped ZnS-SiO<sub>2</sub> nanocomposite with Zn:Mn (98:02, 95:05, 90:10) molar ratios.

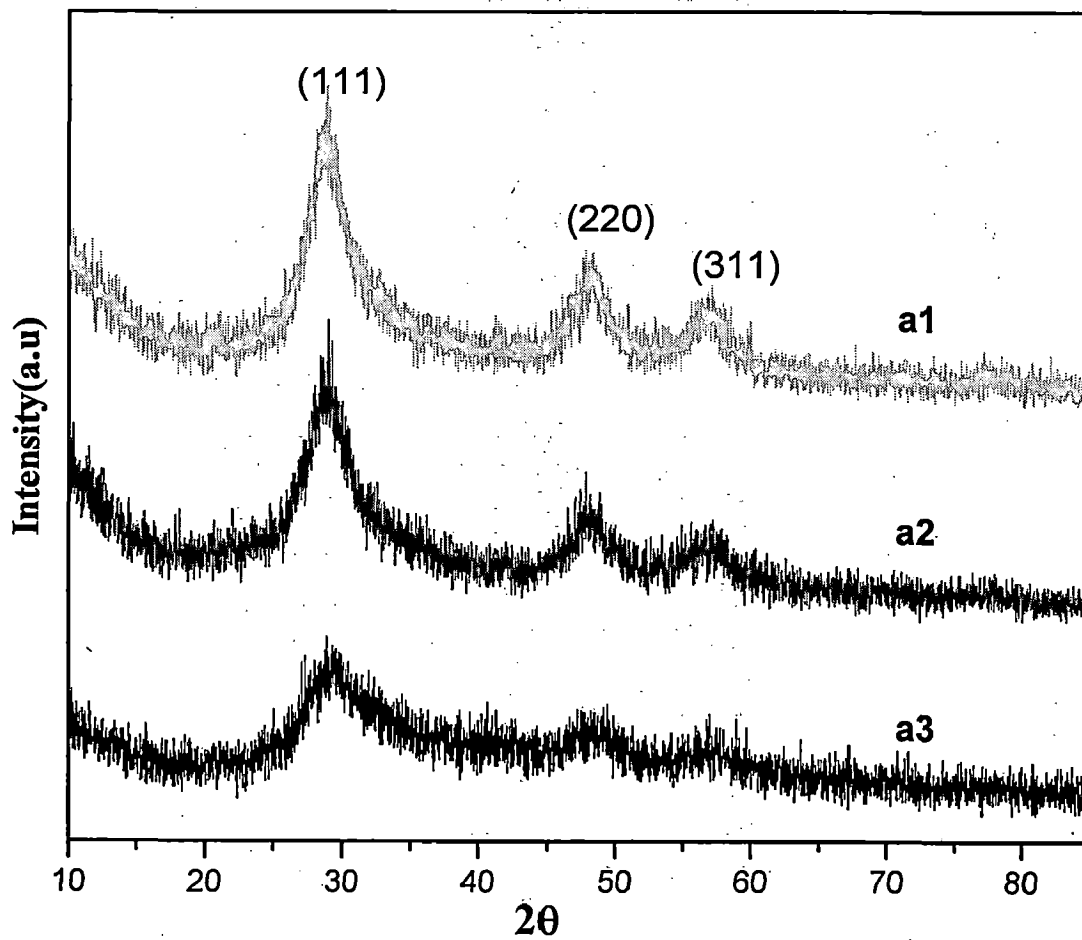


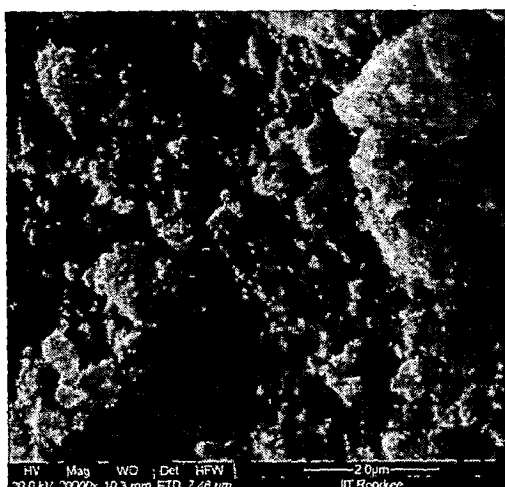
Fig. 4.1.2 XRD patterns of Mn doped ZnS-SiO<sub>2</sub> nanocomposites (a1, a2 and a3) calcined at 400°C.

## ***4.2 FE-SEM images and EDXA analysis of Mn doped ZnS-SiO<sub>2</sub> nanocomposites:***

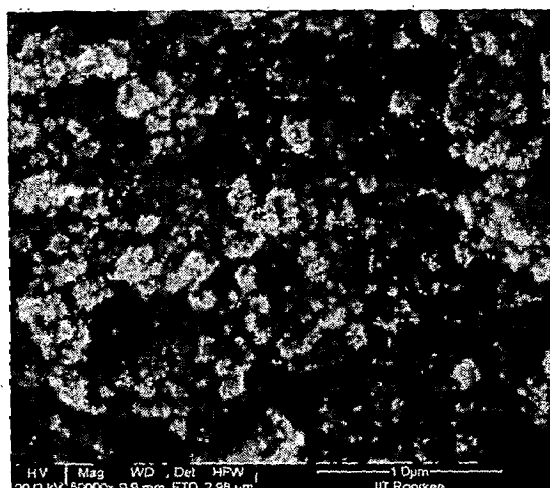
Fig 4.2.1 shows the FE-SEM images of Mn doped ZnS-SiO<sub>2</sub> nanocomposites with different Zn:Mn (98:02 , 95:05, 90:10) molar ratios. In the images of nanocomposites with Zn<sup>2+</sup>:Mn<sup>2+</sup> = 95:05 and 90:10 molar ratios, the nanoparticles are spherical in shape and agglomerated whereas in the case of the nanocomposite with Zn<sup>2+</sup>:Mn<sup>2+</sup> = 98:02 molar ratio, the nanoparticles are with irregular shape.

Fig. 4.2.2 shows the FE-SEM images of Mn doped ZnS-SiO<sub>2</sub> nanocomposites with different Zn:Mn molar ratios (98:02 , 95:05, 90:10) after calcination at 400°C. The morphology of calcined samples are almost same as that of as prepared samples.

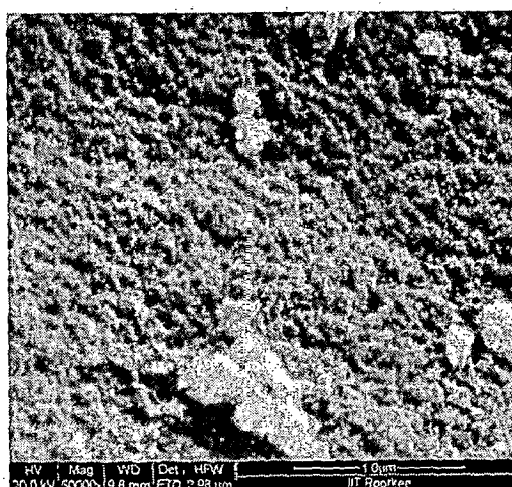




$[Zn^{2+}:Mn^{2+}] = 98:02$



$[Zn^{2+}:Mn^{2+}] = 95:05$



$[Zn^{2+}:Mn^{2+}] = 90:10$

Fig. 4.2.1 FE-SEM images of Mn doped ZnS-SiO<sub>2</sub> nanocomposites with different Zn:Mn molar ratios.

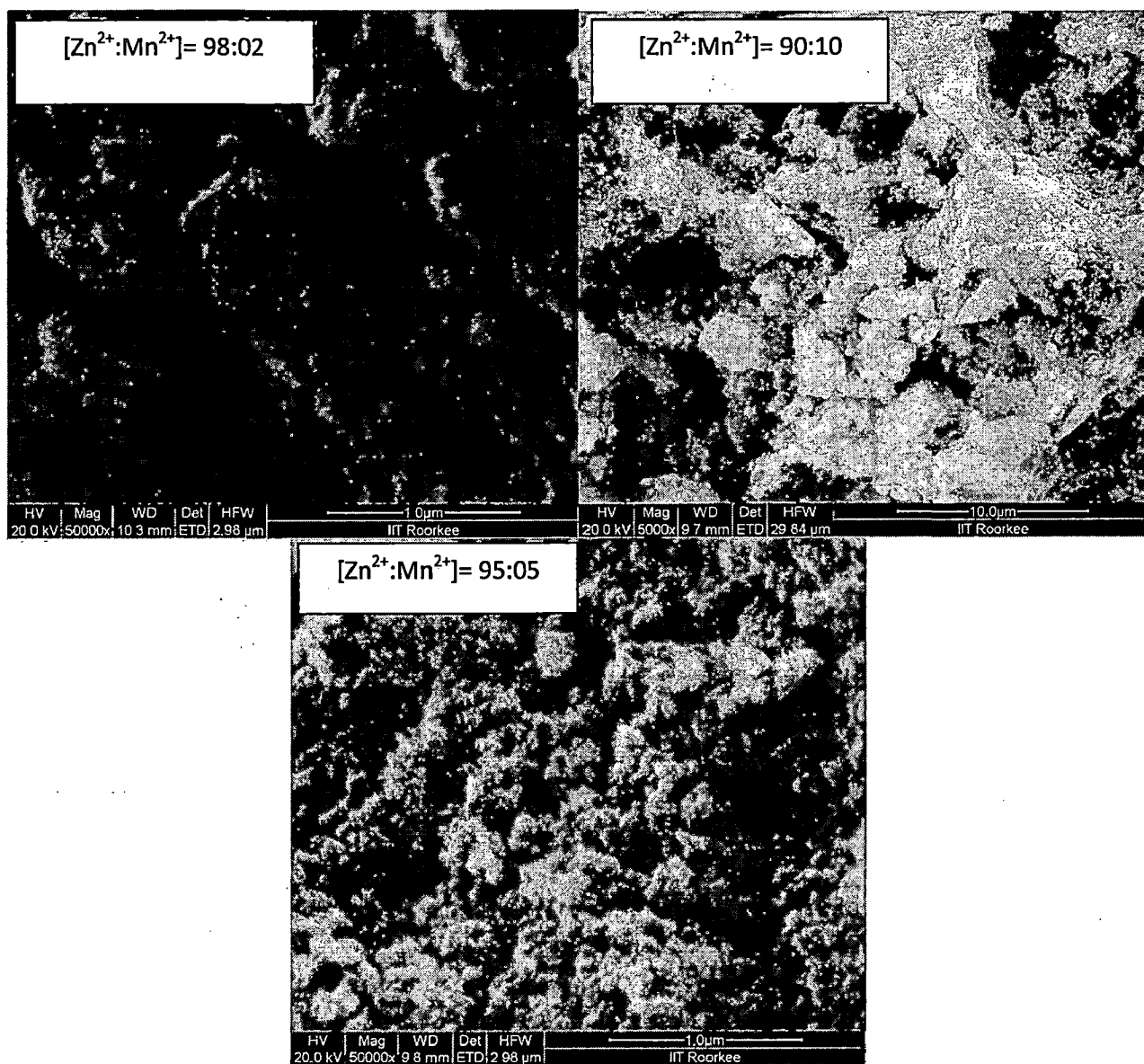
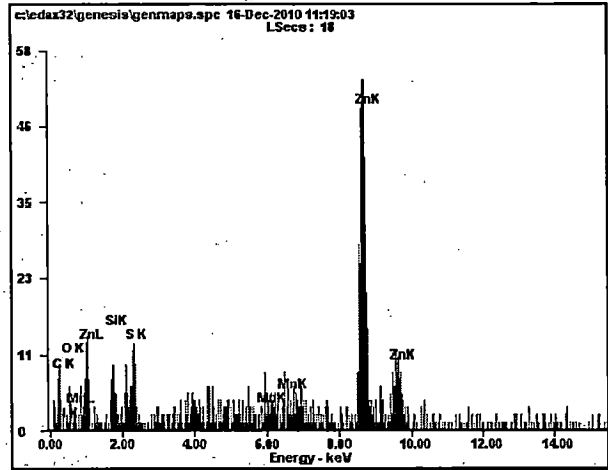
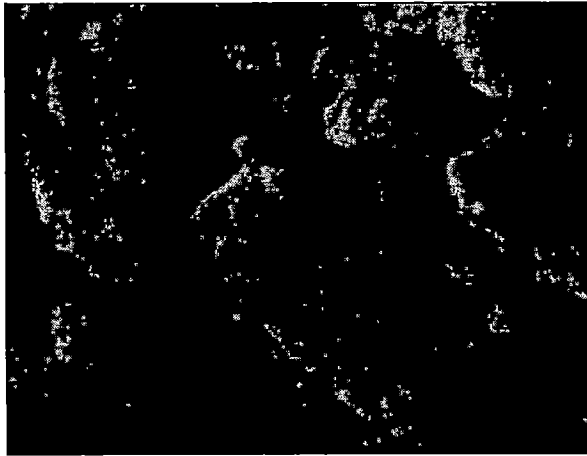


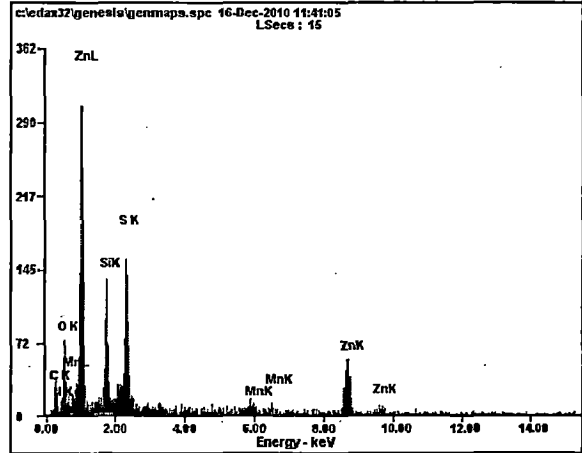
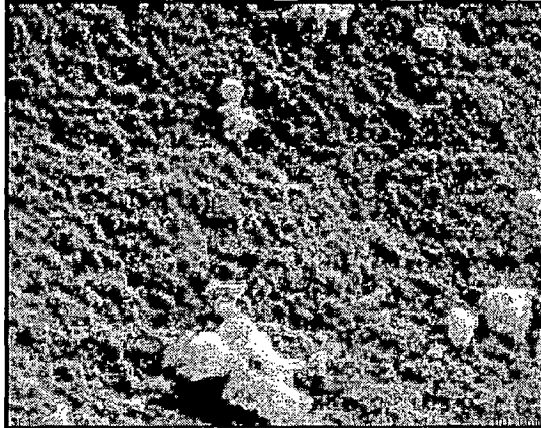
Fig. 4.2.2 FE-SEM images of Mn doped ZnS-SiO<sub>2</sub> nanocomposites with different Zn:Mn molar ratios after calcination at 400°C

The EDXA patterns of Mn doped ZnS-SiO<sub>2</sub> nanocomposites with the lowest loading level and the highest loading level of Zn<sup>2+</sup>:Mn<sup>2+</sup> molar ratios confirmed the presence of Mn, Zn, S, Si and O elements with different weight and atomic percentages (Figures 4.2.3 and 4.2.4).



<i>Element</i>	<i>Wt%</i>	<i>At%</i>
<i>CK</i>	15.03	45.16
<i>NK</i>	01.02	02.63
<i>OK</i>	01.63	03.68
<i>SiK</i>	01.99	02.55
<i>SK</i>	02.40	02.70
<i>MnK</i>	02.47	01.62
<i>ZnK</i>	75.46	41.66
<i>Matrix</i>	Correction	ZAF

Fig. 4.2.3 EDXA data of Mn doped ZnS-SiO<sub>2</sub> nanocomposite with Zn<sup>2+</sup>:Mn<sup>2+</sup> molar ratio of 98:02



<i>Element</i>	<i>Wt%</i>	<i>At%</i>
<i>CK</i>	22.24	45.32
<i>NK</i>	00.00	00.00
<i>OK</i>	12.65	19.36
<i>SiK</i>	10.45	09.10
<i>SK</i>	14.19	10.83
<i>MnK</i>	03.29	01.47
<i>ZnK</i>	37.18	13.92
<i>Matrix</i>	Correction	ZAF

Fig. 4.2.4 EDXA data of Mn doped ZnS-SiO<sub>2</sub> nanocomposite with Zn<sup>2+</sup>:Mn<sup>2+</sup> molar ratio of 90:10

### 4.3 FT-IR spectra of Mn doped ZnS-SiO<sub>2</sub> nanocomposites:

Fig. 4.3.1 shows the FT-IR spectra of ZnS-SiO<sub>2</sub>-2 nanocomposite and Mn doped ZnS-SiO<sub>2</sub> nanocomposites with different Zn<sup>2+</sup>:Mn<sup>2+</sup> (98:02, 95:05, 90:10) molar ratios. The band around 1065 cm<sup>-1</sup> is assigned to Si-O-Si asymmetric stretching where as the band at 791 cm<sup>-1</sup> is due to Si-O-Si symmetric stretching and the band at 460 cm<sup>-1</sup> is due to Si-O-Si bending [44]. The band at 619 cm<sup>-1</sup> is assigned to Zn-S stretching. The band around 3330 cm<sup>-1</sup> in the case of ZnS-SiO<sub>2</sub>-2 and the band around 3430 cm<sup>-1</sup> in the case of Mn doped ZnS-SiO<sub>2</sub> nanocomposites are due to O-H stretching. The band around 1402 cm<sup>-1</sup> is due to OH bending [45, 46].

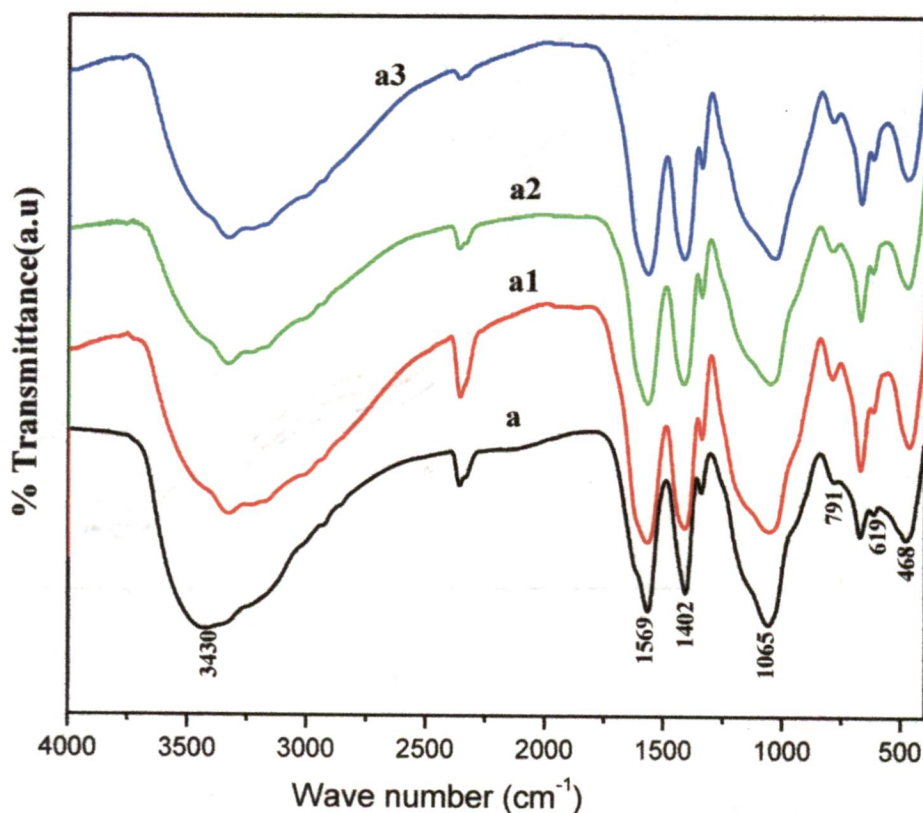


Fig. 4.3.1 FT-IR spectra of (a) ZnS-SiO<sub>2</sub>-2, and Mn doped ZnS-SiO<sub>2</sub> nanocomposites (a1, a2 and a3).

#### 4.4 Thermal gravimetric analysis of Mn doped ZnS-SiO<sub>2</sub> nanocomposites

Fig. 4.4.1 shows the TGA patterns of ZnS-SiO<sub>2</sub>-2 and manganese doped nanocomposites (a1, a2 and a3). In Mn doped ZnS-SiO<sub>2</sub> nanocomposites, the initial loss in weight around 100°C is due to moisture present in the material [50]. The TGA curves of Mn doped ZnS-SiO<sub>2</sub> nanocomposites are similar to that of ZnS-SiO<sub>2</sub> nanocomposites (figure 3.4.1).

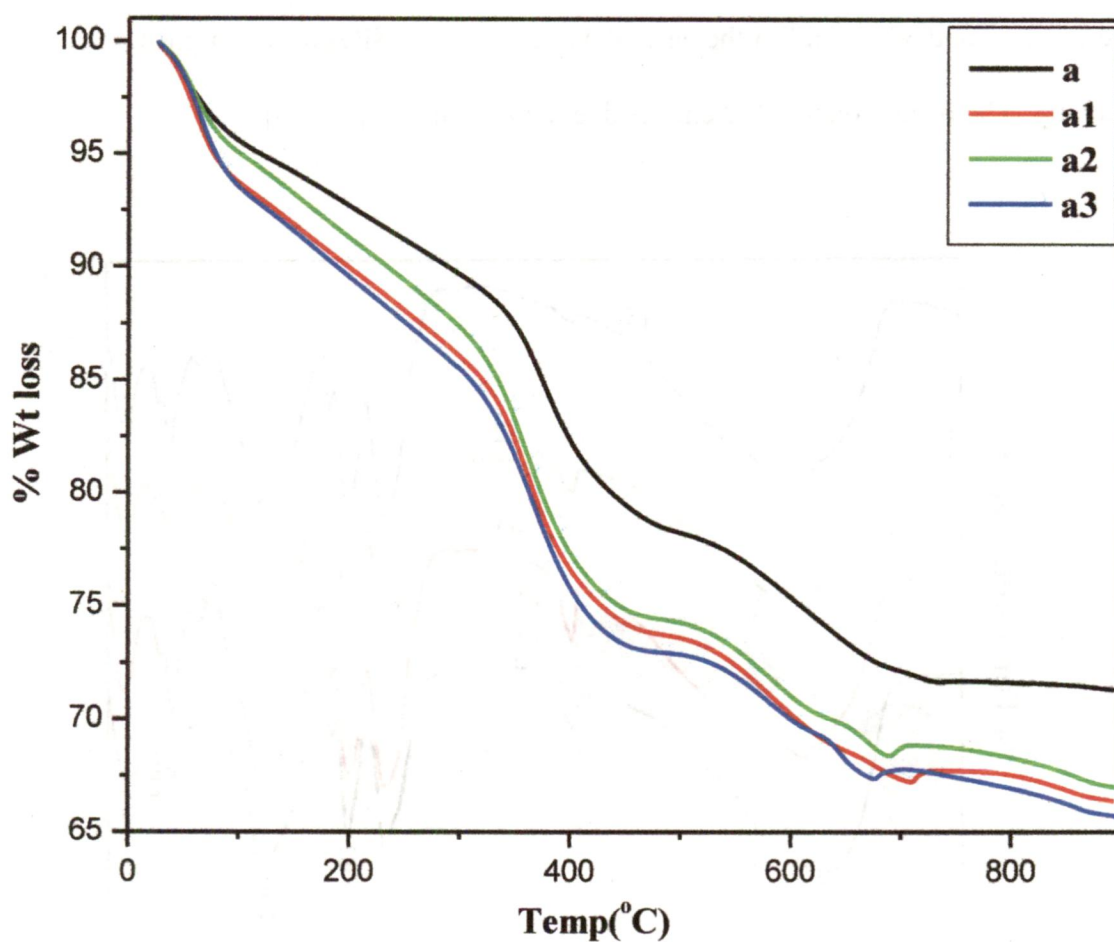


Fig. 4.4.1 TGA patterns of (a) ZnS-SiO<sub>2</sub>-2 and manganese doped ZnS-SiO<sub>2</sub> nanocomposites (a1, a2 and a3)

#### ***4.5 DRS spectra of Mn doped ZnS-SiO<sub>2</sub> nanocomposites:***

Fig. 4.5.1 shows the diffuse reflectance spectra of ZnS-SiO<sub>2</sub>-2 and Mn doped ZnS-SiO<sub>2</sub> nanocomposites with different Zn<sup>2+</sup>: Mn<sup>2+</sup> molar ratios. The calculated bandgap of Mn doped ZnS-SiO<sub>2</sub> nanocomposites with the loading level of Mn (i.e. Zn<sup>2+</sup>: Mn<sup>2+</sup> = 95:05) is 6.2eV whereas in the cases of lowest and highest loading level of Mn (i.e. Zn<sup>2+</sup>: Mn<sup>2+</sup> = 98:02 and 90:10), the bandgap was estimated to be about 7.4 eV (Figure 4.5.2). The bandgap of Mn doped ZnS-SiO<sub>2</sub> nanocomposites with different Zn<sup>2+</sup>: Mn<sup>2+</sup> mole ratios are higher than the ZnS-SiO<sub>2</sub> nanocomposites with variable SiO<sub>2</sub> ratios. The bandgap in ZnS-SiO<sub>2</sub> nanocomposites varies from 4.4 eV to 5.2 eV.

The crystallite size of ZnS in ZnS-SiO<sub>2</sub> nanocomposites and Mn doped ZnS-SiO<sub>2</sub> nanocomposites is decreased in comparison to pure ZnS. The increase in the bandgap in the case of ZnS-SiO<sub>2</sub> nanocomposites compared to pure ZnS nanoparticles is attributed to the smaller crystallites in the case of nanocomposites.

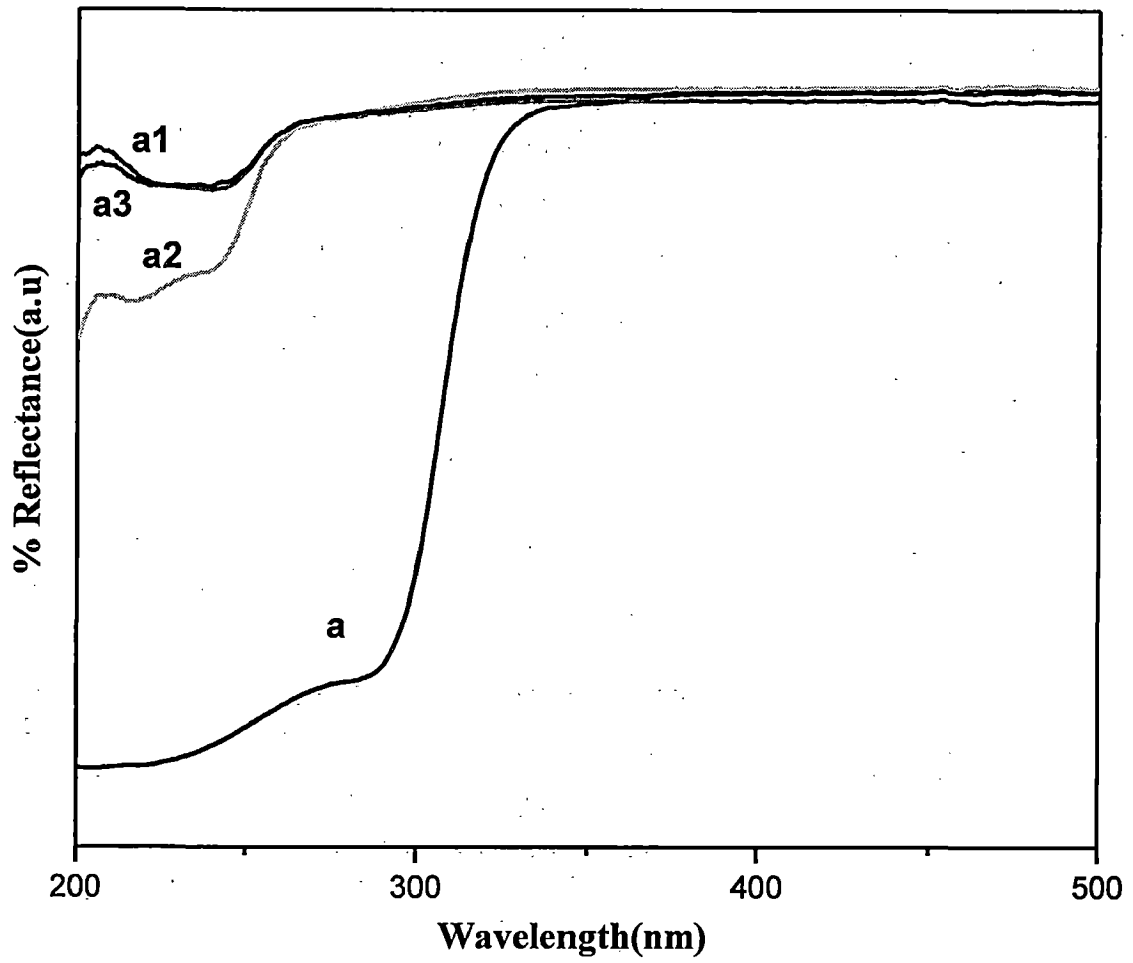


Fig. 4.5.1 DRS spectra of (a) ZnS-SiO<sub>2</sub>-2 and Mn doped ZnS-SiO<sub>2</sub> nanocomposites (a1, a2 and a3).



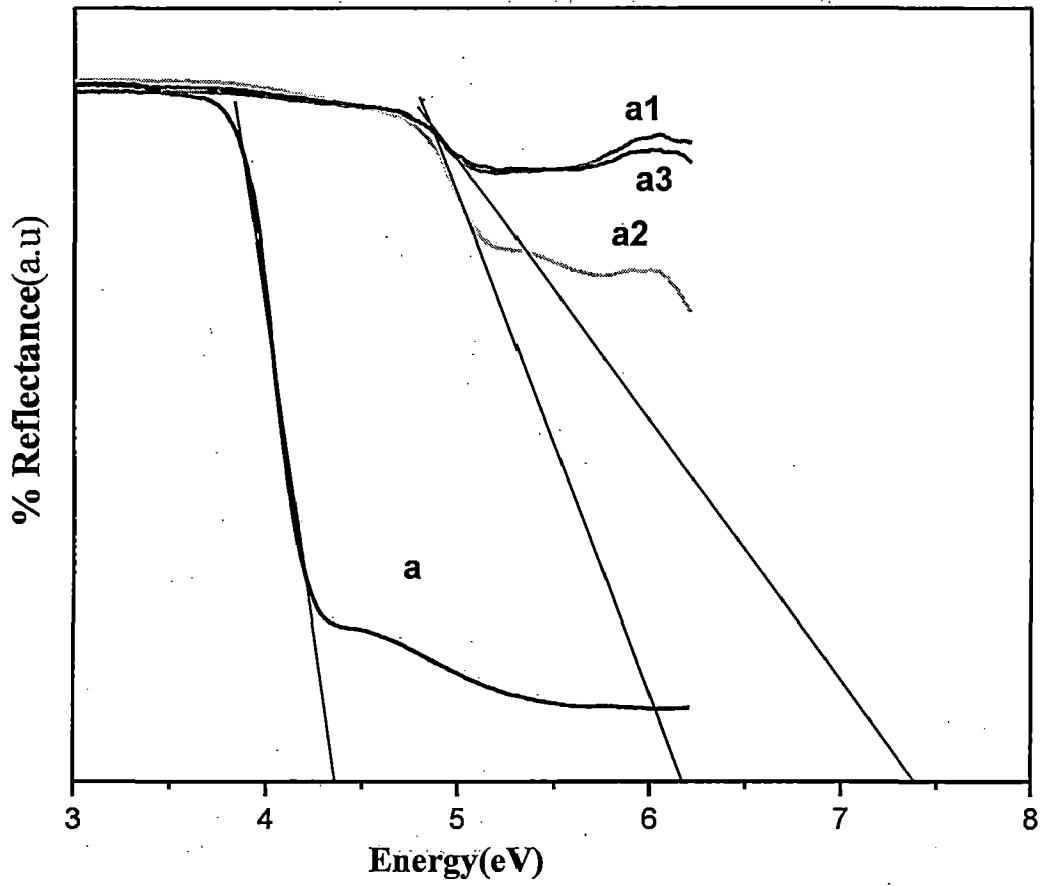


Fig. 4.5.2 DRS spectra of (a) ZnS-SiO<sub>2</sub>-2 and Mn doped ZnS-SiO<sub>2</sub> nanocomposites (a1, a2 and a3).

#### ***4.6 PL spectra of Mn doped ZnS-SiO<sub>2</sub> nanocomposites:***

Fig. 4.6.1 shows the photoluminescence spectra of Mn doped ZnS-SiO<sub>2</sub> nanocomposites with different Zn<sup>2+</sup>:Mn<sup>2+</sup> molar ratios. The photoluminescence spectra were recorded at an excitation wavelength of 325 nm. There are five emission bands located at about 362 nm, 389 nm, 469 nm, 506 nm and 565 nm. The band around 362 nm is assigned due to the impurity in methanol which was used as the solvent during the measurements. The band around 389 nm is assigned due to zinc vacancies in a1, a2 and a3 samples whereas the band at 469 nm is caused by sulphur bondings [48]. The PL at about 506 nm occurs as the electrons are transmitted from the energy level of sulfur vacancies to the energy level of zinc vacancies [47, 52]. The PL peak around 565 nm is assigned as emission due to Mn<sup>2+</sup> doping in ZnS-SiO<sub>2</sub> nanocomposites [47].

Fig. 4.6.2 shows the photoluminescence spectra of Mn doped ZnS-SiO<sub>2</sub> nanocomposites with different Zn<sup>2+</sup>:Mn<sup>2+</sup> molar ratios after calcination at 400°C. The PL spectra were recorded using 325 nm as the excitation. Same emission bands are observed as in the case of uncalcined samples but they are shifted towards blue [45, 47].

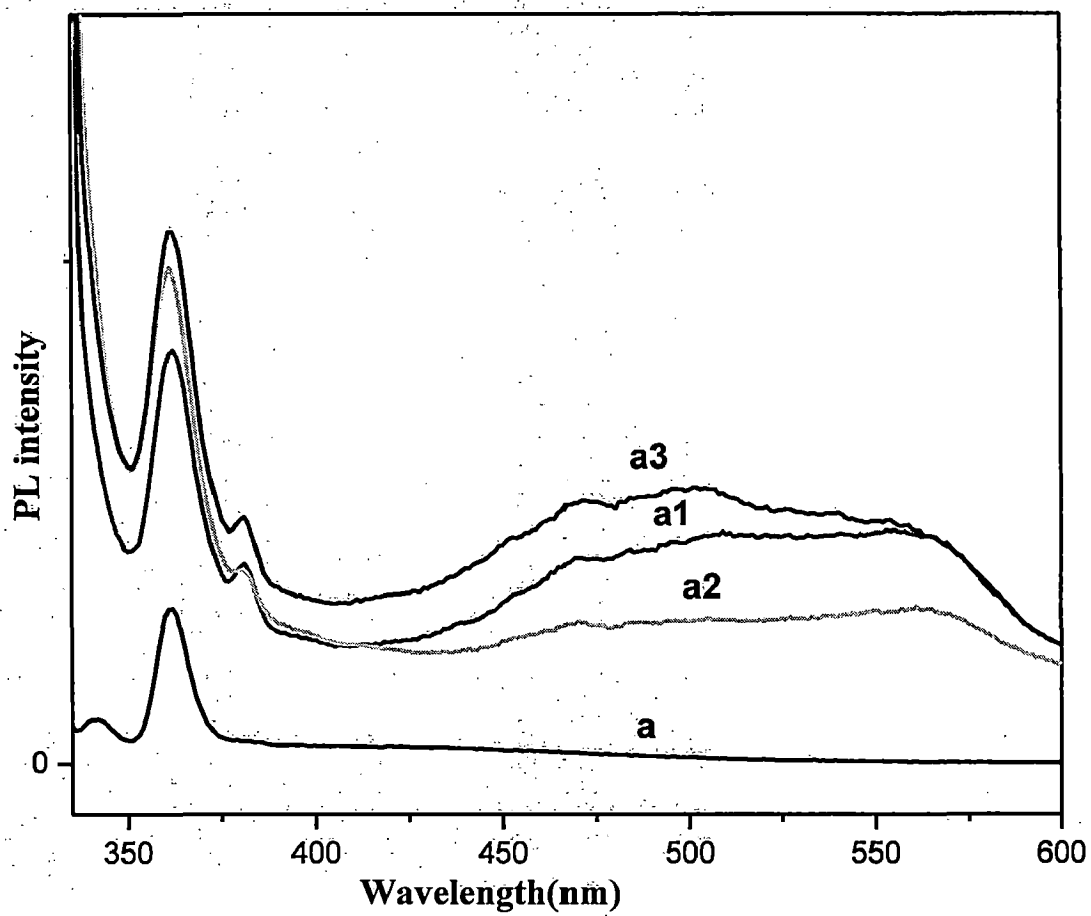


Fig. 4.6.1 PL spectra of manganese doped ZnS-SiO<sub>2</sub> nanocomposites (a1, a2 and a3) and (a) methanol.

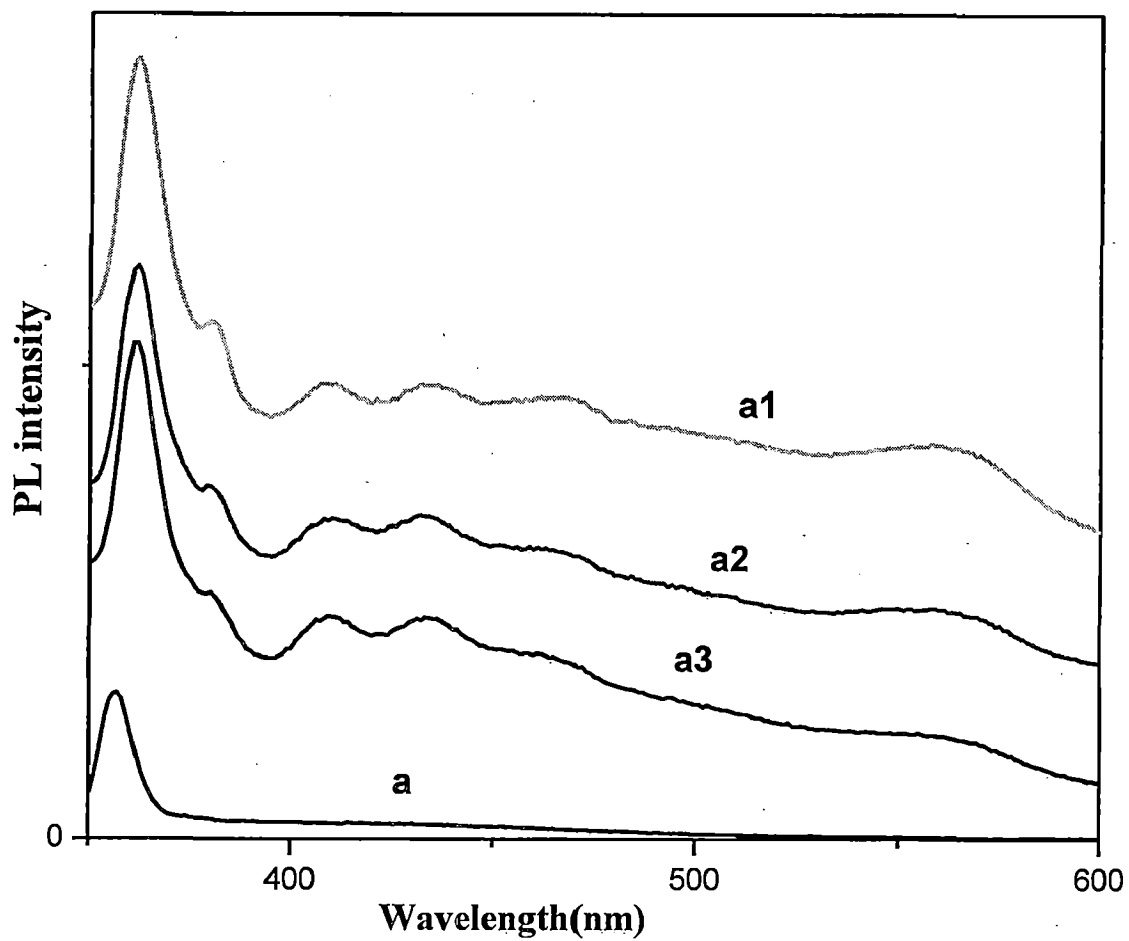


Fig. 4.6.2 PL spectra of manganese doped ZnS-SiO<sub>2</sub> nanocomposites (a1, a2 and a3) calcined at 400°C and the spectrum of methanol (a) is also shown



*Chapter 5*

*Conclusions*

## CHAPTER 5

### **CONCLUSIONS:**

ZnS-SiO<sub>2</sub> nanocomposites with different SiO<sub>2</sub> ratios and Mn doped ZnS-SiO<sub>2</sub> nanocomposites with different Zn<sup>2+</sup>:Mn<sup>2+</sup> molar ratios were synthesized by a simple sol-gel method. It was found that the crystallite size of ZnS in ZnS-SiO<sub>2</sub> nanocomposites and Mn doped ZnS-SiO<sub>2</sub> nanocomposites is decreased in comparison to pure ZnS nanoparticles. The structural and elemental analysis was carried out by powder X-ray diffraction and energy dispersive X-ray analysis. The optical properties of the synthesized ZnS-SiO<sub>2</sub> and Mn doped ZnS-SiO<sub>2</sub> nanocomposites were studied by diffuse reflectance spectroscopy and photoluminescence spectroscopy. It was found that the band gap of Mn doped ZnS-SiO<sub>2</sub> nanocomposites is higher in comparison to pure ZnS nanoparticles and ZnS-SiO<sub>2</sub> nanocomposites.

## REFERENCES:

- 1 P.M. Ajayan, L.S. Schadler, P.V. Braun. *Nanocomposite science and technology*. Wiley (2003).
- 2 L, H.Ying; C, S,Yuan; T, S,Seng; *Journal of Crystal Growth* **269**, 385 (2004).
- 3 Kamigaito, O; *Journal of Japanese Society Powder Metall.* **38**, 315 (1991).
- 4 F. E. Kruis, H. Fissan and A. Peled "Synthesis of nanoparticles in the gas phase for electronic, optical and magnetic applications – a review". *J. Aerosol Sci.* **29**: 511 (1998).
- 5 S. Zhang, D. Sun, Y. Fu and H. Du "Recent advances of superhard nanocomposite coatings: a review". *Surf. Coat. Technol.* **167**: 113 (2003).
- 6 M, Trkula, David O. Harris, *Chemical Physics Letter*, **93**, 4 (1982).
- 7 T. Jung, A. Westphal, *Surface and Coatings Technology*, **59** 171(1993).
- 8 M. Birkholz, U. Albers, and T. Jung. *Surf. Coat. Technol.* **179**: 279 (2004).
- 9 Md, Reza Vaezi, Coupled Semiconductor Metal Oxide Nanocomposites: Types, Synthesis Conditions and Properties. *Advances in Composite Materials for Medicine and Nanotechnology*, p365 (pdf).
- 10 AE. Gash, "*Energetic nanocomposites with sol-gel chemistry: synthesis, safety, and characterization*" (pdf).
- 11 R, R, Kevin; R, G, James; *The Environmentalist* **29**: 56 (2008).
- 12 E, Manias, "Nanocomposites: Stiffer by design". *Nature Materials* **6**: 9 (2007).
- 13 Y. Mai, Z. Yu, Y. Mai, Z. Yu. *Polymer Nanocomposites*. Woodhead Publ (2006).
- 14 T. J. Pinnavaia, G. W. Beall, "*Polymer-Clay Nanocomposites*" Wiley, 2001.

- 15 A, Usuki; M, Kawasum; Y,Kojima; A,Okada; *Journal of Materials Research* **8**: 1174(1993).
- 16 A, Usuki; M, Kawasum; Y,Kojima; A,Okada; *Journal of Materials Research* **8**: 1179 (1993).
- 17 A. B. Morgan, C. A. Wilkie "*Flame Retardant Polymer Nanocomposites*" Wiley, 2007.
- 18 <http://www.nrc-cnrc.gc.ca/eng/ibp/imi/research/polymer-nanocomposites.html>.
- 19 K.J. Yao, M.Song, D.Z.Luo, *Polymer Communication*, **43**, 1017(2002).
- 20 Nicholas A. D. Burke, Harald D. H. Stover, Francis P. Dawson, *Chem. Mater.* **14**, 4752 (2002).
- 21 Y, K, Dong, L,Su Seong, and J, Y. Ying, *Chem. Mater.*, **18**, 2459 (2006).
- 22 <http://www.inframat.com/magnetic.htm>
- 23 A. Lapidus, A. Krylova, V. Kazanskii, V. Borovkov and A. Zaitsev. *Applied Catalysis*, **73**, 6 5 (1991).
- 24 M. Pannirselvam, A.Genovese, M.C Jollands,S.N.Bhattachrya, *eXPRESS Polymer Letter*, **2**, 429 (2008).
- 25 L. A. Acquarulo, Jr. & O'Neil, C.J. (2002, May). *Enhancing medical device with nanocompositepolymers*; <http://www.devicelink.com/mddi/archive/02/05/00.html>
- 26 M, C Henriette. de Azeredo, *Food Research International* **42**: 1240 (2009).
- 27 <http://www.rtpcompany.com/info/flyers/nano.pdf>
- 28 [http://www.epa.gov/opptintr/nano/p2docs/casestudy2\\_lan.pdf](http://www.epa.gov/opptintr/nano/p2docs/casestudy2_lan.pdf)
- 29 J. Musil, *Surf. Coat. Technol.* **125**, 322(2000).
- 30 ] .S. Zhang, D. Sun, Y.Q. Fu, H. J. Du, *Surf. Coat. Technol* , **167**, 113 (2003).



- 31 F. Vaz, L. Rebouta, *Mater. Sci. Forum* **383**, 14 (2002).
- 32 Maurizio Avella, Jan J. De Vlieger, Maria Emanuela Erricoa, Sabine Fischer, Paolo Vacca, Maria Grazia Volpe. *Food Chemistry*; **93**: 467 (2005).
- 33 M. Afsharpour, S. Imani and S. Abdolmohammadi, *World Academy of Science, Engineering and Technology* **76** (2011).
- 34 J. W. Gilman, C. L. Jackson, A. B. Morgan, R. Harris, Jr. *Chem. Mater.* **12**, 1866 (2000).
- 35 J. W. Gilman, *Applied Clay Science* **15**, 31 (1999).
- 36 D. Sridevi, K.V.Rajendran, *Chalcogenide Letters*, **7**, 397 (2010).
- 37 P. R. F. Barnes; R. Mulvaney; E. W. Wolff; K. A. Robinson, *Journal of Microscopy* **205**: 118 (2002).
- 38 <http://www.scribd.com/doc/10514060/Fluorescence-Spectrophotometry>.
- 39 A.W. Coats, J. P. Redfern, *Analyst*, **88**, 906 (1963).
- 40 M. Chu, Y. Sun, S. Xu, *J Nanopart Res* **10**:613 (2008).
- 41 N. Taghavinia, T. Ya. *Physica E*, **21** 96 (2004).
- 42 Nina I. Kovtyukhova, Eugenia V. Buzaneva, Chad C. Waraksa, Benjamin R. Martin, Thomas E. Mallouk, *Chem. Mater.*, **12**, 383 (2000).
- 43 Tianyou Zhai, Zhanjun Gu, Yang Dong, Haizheng Zhong, Ying Ma, Hongbing Fu, Yongfang Li, Jiannian Yao, *J. Phys. Chem. C*, **111** , 11604 (2007).
- 44 M. Navaneethan; J. Archana; K. D. NishA; Y. Hayakawa; S. Ponnusamy; C. Muthamizhchelvan, *Journal of Alloys and Compounds*, **506**, 249 (2010).
- 45 W. Stober, A. Fionk, E. Bohn; *J. Colloid Interface Sci.* **236**, 62(1968).
- 46 K.C. Baric et al., *Journal of Noncrystalline solids* **356**, 153 (2010)

- 47 B.Steit, Y.Axmänn, H.Hofmann,F. Petri, *Journal of Luminescence*, **128**, 92 (2008).
- 48 J. Yang, J.Cao, L.yang,Y. Zhang, J. Lang,; *Journal of Applied Physics*, **108**, 044304 (2010).
- 49 N. Karar, Suchitra Raj, F. Singh, *Journal of Crystal Growth*, **268**, 585 (2004).
- 50 L. H. Ying; C. S.Yuan; T. S. Seng, *Journal of Crystal growth*, **269**,385 (2004).
- 51 A.V.Capilla; R.A Aranda; *Crystal Structure Communications* **8**: 795 (1979).